

000 001 002 003 004 005 006 007 008 009 010 011 012 013 014 015 016 017 018 019 020 021 022 023 024 025 026 027 028 029 030 031 032 033 034 035 036 037 038 039 040 041 042 043 044 045 046 047 048 049 050 051 052 053 VISUAL MULTI-AGENT SYSTEM: MITIGATING HAL- LUCINATION SNOWBALLING VIA VISUAL FLOW

Anonymous authors

Paper under double-blind review

ABSTRACT

Multi-Agent System (MAS) powered by Visual Language Models (VLMs) enables challenging tasks but suffers from a novel failure term, *multi-agent visual hallucination snowballing*, where hallucinations are seeded in a single agent and amplified by following ones due to the over-reliance on textual flow to relay visual information. Through turn-, layer-, and token-wise attention analyses, we provide detailed insights into the essence of hallucination snowballing regarding the reduction of visual attention allocation. It leads us to identify a subset of vision tokens with a unimodal attention peak in middle layers that best preserve visual evidence but gradually diminish in deeper agent turns, resulting in the visual hallucination snowballing in MAS. Thus, we propose **ViF**, a lightweight, model-agnostic mitigation paradigm that relays inter-agent messages with **Visual Flow** powered by the selected visual relay tokens and applies attention reallocation to amplify this pattern. The experiment results demonstrate that our method markedly reduces hallucination snowballing, consistently improving the performance across eight benchmarks based on four common MAS structures and ten base models. The source code will be publicly available.

1 INTRODUCTION

MAS equipped with advanced VLMs are rapidly emerging as a solution for complex tasks, such as collaborative reasoning, multi-turn instruction following, and sophisticated multi-modal understanding, by enabling agents to communicate and collaborate over multiple turns so as to tackle problems that are intractable for a single model (Cemri et al., 2025; Li et al., 2025b). However, this collaboration also exposes a fundamental reliability failure due to the problem of *multi-agent visual hallucination snowballing*, that is, visual misinterpretations or over-preference to textual messages in previous agents that are amplified as information flows through subsequent agents, producing propagatively hallucinated outputs about the visual contents and, ultimately, catastrophic hallucination snowballing. This introduces new reliability and effectiveness challenges in VLM-based MAS that can not be addressed by single-agent research.

It is noteworthy that the visual hallucination snowballing phenomenon in MAS is essentially different from such problem discussed in the previous works (Zhang et al., 2024b; Zhong et al., 2024), given that the hallucination snowballing arises from two distinct but interacting mechanisms, as shown in Figure 1a: (1) intrinsic hallucination, where individual VLM-based agent produces erroneous textual descriptions or assertions about visual contents, and (2) hallucination propagation, where the *over-reliance on textual information flow*, *i.e.*, the generated text, compresses and selectively emphasizes visual features, allowing surviving hallucinated assertions to be treated as authoritative by downstream agents. Since later agents typically accept prior textual context as strong evidence, early hallucinations are hence amplified rather than corrected, producing a snowballing effect across turns. Due to the interaction between these two mechanisms, reducing per-agent hallucination alone, as focused by previous works (Wang et al., 2025; Tang et al., 2025b; Yin et al., 2025; Li et al., 2025c; Zou et al., 2025; Tang et al., 2025a), cannot fully solve the hallucination propagation problem, thus failing to prevent multi-agent hallucination snowballing.

To diagnose how multi-agent pipelines lose visual fidelity across turns, we first conduct a set of preliminary analyses that dissect attention dynamics among turn-wise, layer-wise, and token-wise, through which we empirically conclude that the hallucination snowballing can be evident by the reduction of attention allocated to vision tokens over agent turns, as indicated in Figure 1b and

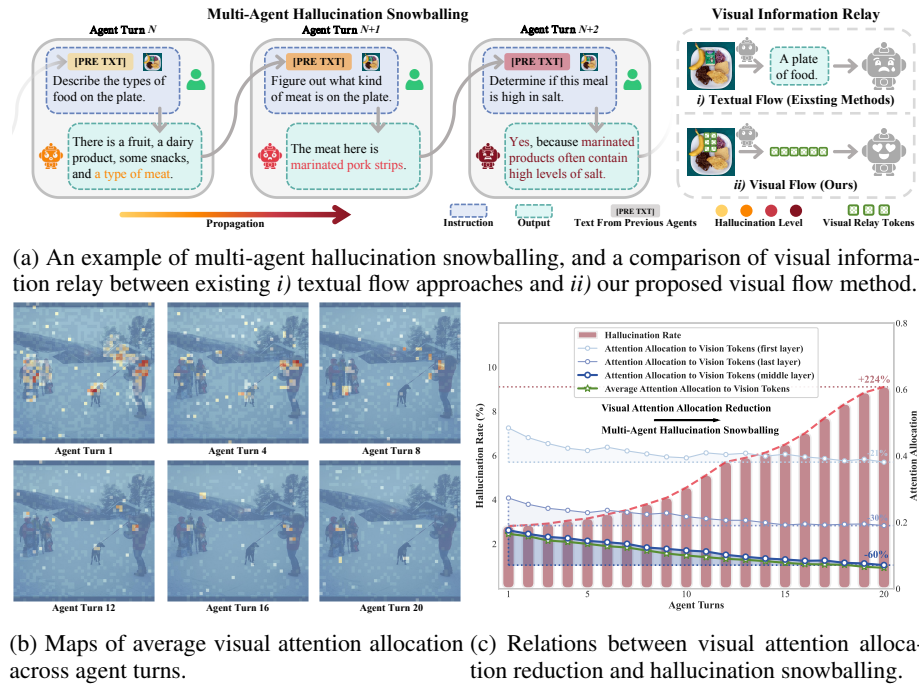


Figure 1: Introduction to the multi-agent visual hallucination snowballing phenomenon: (a) presents an example illustrating how it happens; (b) and (c) specify the visual attention allocation reduction in different agent turns, potentially contributing to the occurrence of hallucination snowballing.

Figure 1c. Moreover, vision tokens characterized by **unimodal attention peak in middle layers**, as a small but vital subset of all vision tokens, can best preserve vision-specific information and whose removal most degrades visual understanding, thus being significant for enhancing the visual information flow among agents. Such a token pattern, however, diminishes in deeper agent turns, implying the gradual dominance of textual information flow, leading to the hallucination snowballing.

Motivated by these insights, we propose an **innovative a plug-and-play** mitigation strategy for multi-agent hallucination snowballing dubbed as ViF. Instead of relying solely on textual flows, an additional **visual flow** is introduced to relay visual evidence by selecting a subset of visual relay tokens and being contextualized by previous instructions, then engaging them in the process of following agents. Such a design can provide downstream agents with preserved visual evidence that resists visual-to-text information loss, meanwhile preventing textual priors from entirely displacing visual signals during subsequent agent turns. In addition, an attention reallocation mechanism is introduced to amplify the ideal attention patterns and preserve visual contributions into deeper agent turns. We evaluate ViF across eight benchmarks covering both comprehensive and hallucination tasks, demonstrating its striking effectiveness in alleviating hallucination snowballing in four different structures and ten base VLMs. Overall, our contributions are summarized as follows:

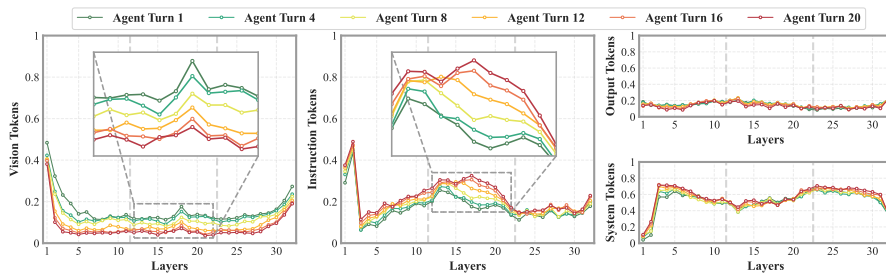
- We formalize the multi-agent visual hallucination snowballing phenomenon and systematically link it to visual attention degradation in deeper agent turns.
- We provide extensive analyses that identify a subset of vision tokens that are critical for relaying visual information flow.
- We introduce ViF, a **model-agnostic plug-and-play** method that optimizes inter-agent visual messages with visual flows and an attention reallocation mechanism to augment attention patterns.
- Comprehensive experiments validate the efficacy of our ViF to reduce hallucination snowballing, and additional analyses provide more convincing evidences.

108 2 REQUISITE ANALYSES

110 As mentioned in Section 1, the hallucination snowballing can be presented by the negative correlation
 111 with the attention allocation to vision tokens. Quantitatively, as shown in Fig. 1c, the average
 112 attention allocation to vision tokens reduces from 0.165 to 0.099 at the 10th agent turn, and further
 113 to 0.063 at the 20th turn, with a total 62% reduction. Furthermore, the reduction in the middle layer
 114 (-60%) is much more remarkable than that in the first (-21%) and last (-30%) layers. For more thor-
 115ough understanding, we conduct extensive requisite analyses among various VLMs. For simplicity,
 116 we mainly focus on LLaVA-NeXT-7B (Liu et al., 2024b) on the POPE (Li et al., 2023) benchmark in
 117 the main paper, while Appendix B provides more detailed settings and comprehensive results on six
 118 VLMs to support the generalization ability of our claims, from which several insights are derived,
 119 thus leading to our research motivations.

120 2.1 ANALYTICAL EXPERIMENTS

122 **Layer-Wise Attention Allocation in Different Agent Turns.** To find out the underlying cause of
 123 visual hallucination snowballing in MAS, we begin by measuring the trend of layer-wise attention
 124 allocation among different agent turns. In VLMs with multi-modal architectures, the decoder dy-
 125namically allocates attention to three types of textual tokens (instruction, system and output tokens)
 126 and one visual token that produced by visual encoder. Other special tokens, such as start and end
 127 signals of visual input, are negligible and thus excluded.



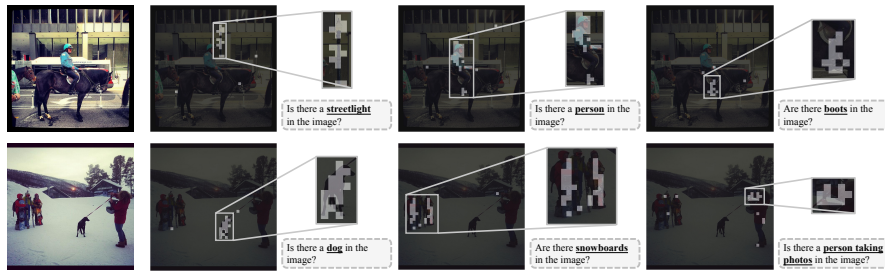
138 Figure 2: Layer-wise attention allocation of four tokens in different agent turns.

140 As depicted in Figure 2, in general, when the agent turns increase, vision tokens receive gradually
 141 decreasing attention in all layers, while the attention being directed towards instruction tokens is
 142 raised accordingly; the attention allocations to system token and output token are relatively stable,
 143 without discernible trend of change. Focusing further on the middle layers of visual and instruction
 144 tokens, which are zoomed in, the opposite trend between visual and instruction tokens is more
 145 pronounced than other layers. In the first agent turn, a scenario equivalent to a single-agent setting,
 146 there exists an obvious unimodal morphology peak in vision attention, and allocation to instruction is
 147 reduced conversely. However, in the 20th turn, the vision attention peak has almost disappeared and
 148 evolved into a fluctuation, and is redistributed to instruction tokens. Based on previous research (Yin
 149 et al., 2025; Zhang et al., 2025c) that textual and visual information are mainly fused and interacted
 150 in these layers, this tendency of attention in MAS suggests that agents in later turns tend to largely
 151 ignore the vision tokens and over-rely on the instruction tokens, including visual contents relayed
 152 by textual output from previous agents. This preference for textual tokens, however, partially leads
 153 to the multi-agent hallucination snowballing. The previous agent may experience visual-to-text
 154 information loss and potential cognitive bias when relaying visual evidence through textual flow.
 155 Conversely, vision tokens, as the initial visual semantic carrier, contain native and unbiased visual
 156 messages, which reduces the potential for hallucinations when relaying visual information. Based
 157 on these observations, we hypothesize: *Can a subset of vision tokens, acting as visual flow, directly
 158 relay visual information across agent turns?*

159 **Dropping Subsets of Vision Tokens in Different Layers.** To intuitively verify the hypothesis,
 160 we ablate specific subsets of vision tokens in shallow/middle/deep layers (implementation modified
 161 from (Zhang et al., 2025b)) and compare the corresponding performance degradation. We choose
 162 five subsets of vision tokens to ablate: (1) Random Tokens: randomly select tokens from the whole
 163 vision token set and maintain a relatively uniform distribution in the image. (2) Inactive Tokens:

162 Table 1: Results of dropping vision token subsets in the shallow, middle, and deep layers.
163

	Shallow Layers				Middle Layers				Deep Layers			
	25%	50%	75%	100%	25%	50%	75%	100%	25%	50%	75%	100%
w/o Dropping	85.2											
(a) Random	51.8	43.4	44.5	40.7	38.4	46.8	30.5	54.7	78.9	6.3	66.1	19.1
(b) Inactive	55.1	430.1	46.2	439.0	41.8	43.4	32.5	52.7	84.3	0.9	82.9	2.3
(c) Rise	41.9	44.3	35.6	49.6	29.6	55.6	20.8	164.4	79.4	5.8	64.2	21.0
(d) Fall	41.6	44.3	36.6	46.4	30.7	54.5	22.5	62.7	78.3	6.9	64.8	20.4
(e) Unimodal	42.1	44.1	37.6	47.6	30.0	55.2	22.8	62.4	52.9	32.3	44.5	40.7

171 Figure 4: The demonstrations of selected unimodal vision tokens in various cases.
172
173
174
175
176
177
178
179

180 select the tokens with constantly low attention and tiny fluctuation. (3) Rise Tokens and (4) Fall
181 Tokens: select tokens allocated with a gradually upward or downward trend of attention. (5) **Uni-**
182 **modal Tokens**: select tokens allocated with an unimodal attention peak. In terms of the unimodal
183 tokens, we introduce a parameter ω to regulate the salience of the attention peak.

184 As listed in Table 1, the ablation of vision tokens leads to varying degrees of
185 performance degradation across layers. In shallow layers, all vision tokens are
186 necessary for the visual understanding capacity; even ablating one-quarter of
187 the tokens from any subset causes over a 30% loss. On the contrary, in the deep
188 layers, vision tokens play an insignificant role, with performance reduction
189 of less than 1% even when dropping all inactive vision tokens. Figure 3 further
190 highlights that, compared to the results of other subsets, the dropping of unimodal
191 tokens in middle layers leads to more significant performance degradation. Specifically,
192 the decrease from this subset is almost three times that of other subsets when dropping
193 one-quarter of the tokens, and about twice when dropping half, three-quarters, and all tokens.
194 In conclusion, the ablation study reveals that in shallow and deep layers,
195 vision tokens are almost equally important or unimportant; however, in the middle layers,
196 vision tokens with unimodal morphology play a much more crucial role in interaction information
197 between vision and text tokens.
198

199 **Investigation of Unimodal Tokens.** To validate our previous hypothesis that certain vision tokens
200 can act as a visual flow for relaying visual information, we visualize the unimodal vision tokens
201 in various cases and track their ratios across agent turns. As demonstrated in Figure 4, we choose
202 two images, each with three distinct questions, as examples. The selected tokens are highly
203 semantically relevant and contain very few other irrelevant tokens. Besides, as depicted in Figure 5,
204 the proportion of unimodal vision tokens continuously declines from 1.22% at the first agent turn
205 to 0.10% at the 20th agent turn, while the percentages of the other two tokens slightly increase.
206 The downward trend of the unimodal token proportion aligns with visual attention allocation among
207 agent turns, which suggests that the reduction of unimodal vision tokens contributes significantly
208 to the onset of hallucination snowballing through the disappearance of the visual attention peak.
209

216 Thus, we believe that
 217 the subset of uni-
 218 modal vision tokens
 219 could meet the hy-
 220 pothesis to relay vi-
 221 sual evidence as vi-
 222 sual flow. It ensures
 223 that semantically rel-
 224 evant visual messages
 225 can be relayed suffi-
 226 ciently, while avoiding carrying substantial irrelevant vision tokens with high efficiency.



Figure 5: Proportions of vision tokens subsets in different agent turns.

227 2.2 INSIGHTS

229 Based on experimental results and analyses, three significant insights can be summarized:

- 231 The visual evidence relayed in MAS, which is typically via textual flow, potentially results
 232 in multi-agent hallucination snowballing.
- 233 When the agent turns increase, the average attention allocated to vision tokens reduces,
 234 and the attention peak in middle layers diminishes, while attention to instruction tokens
 235 increases accordingly; system and output tokens receive relatively stable attention.
- 236 In middle layers, vision tokens with unimodal attention allocation relay visual information;
 237 all vision tokens are significant in shallow layers and less significant in deep layers.

239 3 METHODOLOGIES

241 Building on the insights from the previous section, we propose a straightforward and efficient [model-
 242 agnostic plug-and-play](#) method named ViF to mitigate hallucination snowballing in VLM-based
 243 MAS. As demonstrated in Figure 6, our proposed method involves relaying the visual information
 244 from the previous agent via a selected subset of vision tokens, and reallocating attention in middle
 245 and deep layers to facilitate this process. Besides, we provide a suitable alternative for attention
 246 score based token selection, since in some recently released models with Flash-Attention 2/3 (Dao,
 247 2024), the attention scores are not accessible.

249 3.1 VISUAL INFORMATION RELAY

251 Leveraging the previous insights, we employ the unimodal vision tokens as additional visual flow to
 252 relay information from the previous agent. Specifically, we token-wise decompose the vision tokens
 253 $\mathcal{V} = \{v_1, \dots, v_m\}$ according to the trend of the attention allocation in the middle layers, and select
 254 the vision tokens with unimodal morphology as initial visual relay tokens $\mathcal{R} = \{r_1, \dots, r_n\} \subset \mathcal{V}$,
 255 where $n \ll m$. However, the original selected tokens are semantically irrelevant, which are only
 256 tokenized by the vision encoder, without particular semantics. Thus, we contextualize the initial
 257 visual relay tokens \mathcal{R} with the instruction tokens \mathcal{I} as follows:

$$\widehat{\mathcal{R}} = f(\mathcal{R} \oplus \mathcal{I})[:, n], \quad (1)$$

259 where $f(\cdot)$ is a lightweight transformer block (Mehta et al., 2021), \oplus denotes concatenation. Here,
 260 we extract the former n component to maintain the initial length of visual relay tokens $\widehat{\mathcal{R}}$.

262 To retain the spatial information of visual relay tokens, we apply the same positional encoding
 263 strategy as the previous agent. Then, the visual relay tokens will be transmitted to the subsequent
 264 agent, which will be inserted between the original vision tokens and instruction tokens, and be fed
 265 to the final LLM together with other tokens.

267 3.2 ATTENTION REALLOCATION

268 Considering the insights that tokens are of different significance in the shallow, middle, and deep
 269 layers respectively, we reallocate attention to optimize attention patterns. Our objectives are to

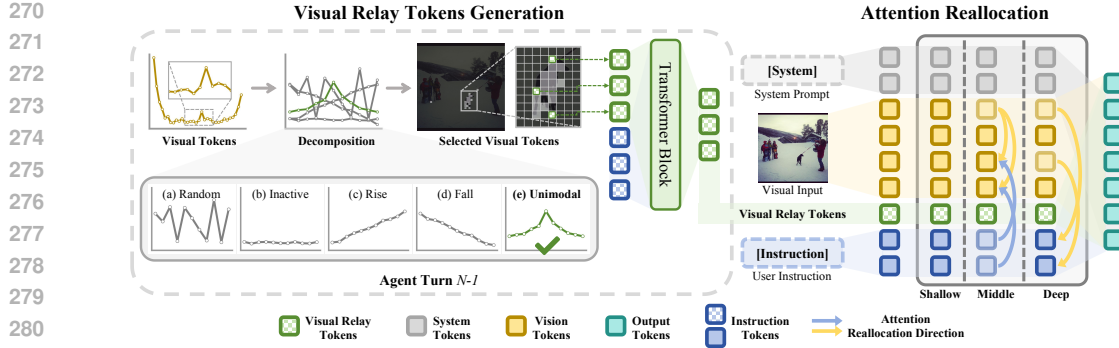


Figure 6: Overview of our proposed ViF, including the generation of visual relay tokens and attention reallocation to alleviate multi-agent hallucination snowballing.

activate the visual relay tokens and to optimize the distribution of attention among various tokens. Therefore, we amplify dynamic trends, both the upward and downward, of visual attention in the middle layers by adding temperature scaling to the Softmax operation in the middle layers:

$$\mathcal{A} = \text{Softmax}_\tau(\mathcal{S}) = \frac{\exp\left(\frac{s}{\tau}\right)}{\sum_{i=1}^m \exp\left(\frac{s_i}{\tau}\right)}, \quad (2)$$

where τ is temperature parameter, \mathcal{S} and s are attention score matrix and attention score, and \mathcal{A} is attention matrix. It promotes the emergence of vision tokens with unimodal morphology. Besides, in the middle layers, we collect the attention of inactive vision tokens and instruction tokens, and then reallocate the collected attention to other vision tokens, which is formulated as:

$$\mathcal{C} = \alpha \sum_{i=1}^m s_i \circ M_c, M_c(i, j) = \mathbb{I}((i \in \mathcal{T}, j \in \mathcal{V}_\emptyset) \vee (i \in \mathcal{T}, j \in \mathcal{I})), \quad (3)$$

$$\hat{s} = s + \frac{s}{\sum_{i=1}^l s_i} \mathcal{C} \circ M_r, M_r(i, j) = \mathbb{I}(i \in \mathcal{T}, j \in \mathcal{V}_\circ), \quad (4)$$

where M_c and M_r are the collection and reallocation mask matrices respectively, which designate the source and destination of the attention reallocation. Besides, α is the reallocation coefficient, \mathcal{T} is the whole token set, $\mathcal{V}_\emptyset \subset \mathcal{V}$ is inactive vision token set, and $\mathcal{V}_\circ = \mathcal{V} - \mathcal{V}_\emptyset = \{v_1, \dots, v_l\}$. During the reallocation, the sum of the total attention is always 1. Additionally, in the deep layers, the reallocation is from vision tokens to instruction tokens, with the same process. Thus, the two mask matrices and the reallocation coefficient are modified correspondingly.

3.3 ALTERNATIVE OF ATTENTION SCORE BASED STRATEGY

To accelerate the computation and reduce memory, flash-attention (Dao, 2024) mechanisms are widely used in recently released models, making the attention scores not obtainable. Inspired by (Wen et al., 2025), we design a Key-Norm (L_2 norm of the key matrix) based alternative for the original attention score based method. More discussions about the alternative are in Appendix C.2.

4 EXPERIMENTS

We conduct experiments on three comprehensive benchmarks: MME (Yin et al., 2024), MM-Bench (Liu et al., 2024d), MM-Vet (Yu et al., 2024), and five visual hallucination benchmarks: CHAIR (Rohrbach et al., 2018), POPE (Li et al., 2023), AMBER (Wang et al., 2023), MMHall-Bench (Sun et al., 2023), HallBench (Guan et al., 2024). Besides, we also include four benchmarks in augmented visual domains: MMIU (Meng et al., 2024), MuirBench (Wang et al., 2024a), MV-Bench (Li et al., 2024), and Video-MME (Fu et al., 2025). For detailed experimental settings, configurations, and additional results, please refer to Appendix D.1 and D.2.

4.1 MAIN RESULTS

Performance on Comprehensive and Hallucination Benchmarks. For comprehensive assessments of our proposed ViF, we first compare the results on six base VLMs, namely, LLaVA-v1.5-

324
 325 Table 2: Results across eight comprehensive and hallucination benchmarks. * indicates implement-
 326 tion with Key-Norm, while others use attention scores. The best and the second best values with
 327 our method are **bolded** and underlined respectively, and the rightmost column shows the average
 328 results. For identical values, we compare the following digit after the decimal point.

MAS Structure	Base Agent	MME↑	MM Bench↑	MM-Vet↑	CHAIR↓	POPE↑	AMBER↑	MMHal-Bench↑	Hall Bench↑	Avg.↑
Linear	LLaVA-v1.5-7B	1516.2	66.1	32.4	52.4	86.7	85.2	40.5	48.0	
	+Ours	1531.8 <u>15.6</u>	67.8 <u>1.7</u>	34.6 <u>2.2</u>	51.7 <u>0.7</u>	88.6 <u>1.9</u>	87.8 <u>2.6</u>	42.8 <u>2.3</u>	50.6 <u>2.6</u>	↑ 3.5%
	LLaVA-v1.6-7B	1511.7	68.7	36.9	45.5	86.7	88.5	43.4	52.6	
	+Ours	1524.3 <u>12.6</u>	69.4 <u>0.7</u>	38.2 <u>1.3</u>	43.6 <u>1.9</u>	88.2 <u>1.5</u>	91.5 <u>3.0</u>	46.0 <u>2.6</u>	54.7 <u>2.1</u>	↑ 3.1%
	LLaVA-NeXT-7B	1567.0	72.1	47.1	44.6	88.6	87.0	45.9	52.9	
	+Ours	1585.2 <u>18.2</u>	73.5 <u>1.4</u>	49.3 <u>2.2</u>	42.9 <u>1.7</u>	90.4 <u>1.8</u>	89.3 <u>2.3</u>	48.1 <u>2.2</u>	55.3 <u>2.4</u>	↑ 3.2%
	LLaVA-OV-7B	1587.6	82.3	58.4	38.3	91.4	91.3	47.8	53.7	
	+Ours*	1598.8 <u>11.2</u>	83.4 <u>1.1</u>	59.9 <u>1.5</u>	37.2 <u>1.1</u>	93.0 <u>1.6</u>	93.9 <u>2.6</u>	49.6 <u>1.8</u>	56.1 <u>2.4</u>	↑ 2.6%
	Qwen2-VL-7B	1686.4	81.9	63.3	38.4	90.5	91.2	48.2	51.9	
	+Ours*	1699.6 <u>13.2</u>	82.4 <u>0.5</u>	65.2 <u>1.9</u>	37.8 <u>0.6</u>	91.7 <u>1.2</u>	94.0 <u>2.8</u>	50.2 <u>2.0</u>	54.4 <u>2.5</u>	↑ 2.4%
	Qwen2.5-VL-7B	1730.4	83.9	67.3	38.6	89.9	92.8	51.6	53.8	
	+Ours*	1746.2 <u>15.8</u>	85.3 <u>1.4</u>	69.1 <u>1.8</u>	37.6 <u>1.0</u>	91.4 <u>1.5</u>	94.4 <u>1.6</u>	53.7 <u>2.1</u>	56.2 <u>2.4</u>	↑ 2.5%
Layered	LLaVA-v1.5-7B	1512.5	63.6	30.6	49.0	86.0	83.5	41.3	46.6	
	+Ours	1520.9 <u>8.4</u>	64.7 <u>1.1</u>	32.0 <u>1.4</u>	49.3 <u>0.3</u>	87.6 <u>1.6</u>	86.1 <u>2.6</u>	43.7 <u>2.4</u>	48.9 <u>2.3</u>	↑ 2.7%
	LLaVA-v1.6-7B	1508.0	66.6	35.1	44.2	86.8	85.2	42.0	48.2	
	+Ours	1518.9 <u>10.9</u>	68.4 <u>1.8</u>	37.5 <u>2.4</u>	42.7 <u>1.5</u>	87.9 <u>1.1</u>	87.1 <u>1.9</u>	43.6 <u>1.6</u>	50.4 <u>2.2</u>	↑ 3.2%
	LLaVA-NeXT-7B	1555.2	69.2	44.0	44.2	87.0	85.6	44.7	49.5	
	+Ours	1571.3 <u>16.1</u>	70.7 <u>1.5</u>	46.5 <u>2.5</u>	42.5 <u>1.7</u>	89.2 <u>2.2</u>	87.7 <u>2.1</u>	47.2 <u>2.5</u>	51.6 <u>2.1</u>	↑ 3.5%
	LLaVA-OV-7B	1584.2	80.6	57.9	37.6	89.9	89.1	45.2	52.7	
	+Ours*	1596.7 <u>12.5</u>	82.0 <u>1.4</u>	59.5 <u>1.6</u>	36.4 <u>1.2</u>	91.5 <u>1.6</u>	90.9 <u>1.8</u>	46.9 <u>1.7</u>	54.5 <u>1.8</u>	↑ 2.5%
	Qwen2-VL-7B	1679.0	79.3	61.5	37.7	88.6	88.5	45.9	49.1	
	+Ours*	1692.6 <u>13.6</u>	80.6 <u>1.3</u>	63.4 <u>1.9</u>	37.1 <u>0.6</u>	90.5 <u>1.9</u>	90.6 <u>2.1</u>	48.1 <u>2.2</u>	50.9 <u>1.8</u>	↑ 2.5%
Random	Qwen2.5-VL-7B	1722.5	81.0	62.1	36.8	87.5	90.1	47.0	51.2	
	+Ours*	1737.0 <u>14.5</u>	82.4 <u>1.4</u>	63.8 <u>1.7</u>	36.0 <u>0.8</u>	89.6 <u>2.1</u>	91.7 <u>1.6</u>	49.3 <u>2.3</u>	53.2 <u>2.0</u>	↑ 2.6%
	LLaVA-v1.5-7B	1519.6	67.1	33.1	49.4	88.3	89.0	44.6	52.8	
	+Ours	1537.6 <u>18.0</u>	68.4 <u>1.3</u>	34.7 <u>1.6</u>	49.8 <u>0.4</u>	90.2 <u>1.9</u>	92.2 <u>3.2</u>	47.0 <u>2.4</u>	55.0 <u>2.2</u>	↑ 2.8%
	LLaVA-v1.6-7B	1519.8	69.0	36.9	43.9	88.6	91.3	44.3	54.9	
	+Ours	1534.4 <u>14.6</u>	69.7 <u>0.7</u>	38.0 <u>1.1</u>	41.8 <u>2.1</u>	89.7 <u>1.1</u>	94.0 <u>2.7</u>	46.8 <u>2.5</u>	57.3 <u>2.4</u>	↑ 3.1%
	LLaVA-NeXT-7B	1576.2	73.0	49.2	43.4	90.4	89.2	47.2	55.4	
	+Ours	1596.1 <u>19.9</u>	75.3 <u>2.3</u>	50.1 <u>0.9</u>	41.6 <u>1.8</u>	93.0 <u>2.6</u>	92.9 <u>3.7</u>	49.3 <u>2.1</u>	58.4 <u>3.0</u>	↑ 3.5%
	LLaVA-OV-7B	1590.1	83.7	58.5	37.7	92.5	91.9	46.3	56.2	
	+Ours*	1605.2 <u>15.1</u>	85.1 <u>1.4</u>	59.7 <u>1.2</u>	37.1 <u>0.6</u>	94.1 <u>1.6</u>	94.9 <u>3.0</u>	48.5 <u>2.2</u>	59.1 <u>2.9</u>	↑ 2.6%
Circular	Qwen2-VL-7B	1690.1	84.1	64.4	38.1	90.8	92.3	46.5	53.7	
	+Ours*	1703.1 <u>13.0</u>	84.9 <u>0.8</u>	65.2 <u>0.8</u>	37.2 <u>0.9</u>	92.7 <u>1.9</u>	95.4 <u>3.1</u>	48.4 <u>1.9</u>	56.3 <u>2.6</u>	↑ 2.5%
	Qwen2.5-VL-7B	1737.7	86.5	67.0	37.8	90.4	93.6	48.9	56.8	
	+Ours*	1756.8 <u>19.1</u>	88.4 <u>1.9</u>	68.1 <u>1.1</u>	37.0 <u>0.8</u>	92.8 <u>2.4</u>	95.8 <u>2.2</u>	50.6 <u>1.7</u>	59.5 <u>2.7</u>	↑ 2.5%
	LLaVA-v1.5-7B	1520.9	67.9	33.5	52.7	88.9	88.7	42.4	51.7	
	+Ours	1539.1 <u>18.2</u>	68.4 <u>0.5</u>	36.0 <u>2.5</u>	51.3 <u>1.4</u>	90.4 <u>1.5</u>	91.6 <u>2.9</u>	44.7 <u>2.3</u>	54.1 <u>2.4</u>	↑ 3.4%
	LLaVA-v1.6-7B	1519.5	69.7	37.7	42.7	88.5	91.2	43.4	53.8	
	+Ours	1537.1 <u>17.6</u>	71.3 <u>1.6</u>	39.3 <u>1.6</u>	40.7 <u>2.0</u>	90.1 <u>1.6</u>	93.8 <u>2.6</u>	46.0 <u>2.6</u>	56.1 <u>2.3</u>	↑ 3.5%
	LLaVA-NeXT-7B	1580.5	73.2	49.5	43.0	91.0	89.4	47.9	53.1	
	+Ours	1599.5 <u>19.0</u>	74.6 <u>1.4</u>	51.8 <u>2.3</u>	41.2 <u>1.8</u>	93.3 <u>2.3</u>	92.7 <u>3.3</u>	51.1 <u>3.2</u>	55.7 <u>2.6</u>	↑ 3.8%
	LLaVA-OV-7B	1592.8	84.0	59.1	38.7	92.8	92.2	47.3	54.6	
	+Ours*	1606.1 <u>13.3</u>	84.6 <u>0.6</u>	60.2 <u>1.1</u>	36.9 <u>1.8</u>	94.0 <u>1.2</u>	95.0 <u>2.8</u>	49.4 <u>2.1</u>	56.9 <u>2.3</u>	↑ 2.7%
	Qwen2-VL-7B	1692.8	83.3	63.9	38.1	91.6	92.8	47.7	52.4	
	+Ours*	1706.3 <u>13.5</u>	84.1 <u>0.8</u>	65.1 <u>1.2</u>	37.2 <u>0.9</u>	93.3 <u>1.7</u>	94.8 <u>2.0</u>	50.2 <u>2.5</u>	54.6 <u>2.2</u>	↑ 2.4%
	Qwen2.5-VL-7B	1738.1	85.2	66.7	38.2	91.3	93.5	50.1	54.9	
	+Ours*	1756.2 <u>18.1</u>	86.6 <u>1.4</u>	68.1 <u>1.4</u>	37.4 <u>0.8</u>	93.4 <u>2.1</u>	95.9 <u>2.4</u>	52.5 <u>2.4</u>	57.3 <u>2.4</u>	↑ 2.6%

Table 3: Results of larger-size models on circular MAS structure.

Base Agent	MME↑	MM Bench↑	MM-Vet↑	CHAIR↓	POPE↑	AMBER↑	MMHal-Bench↑	Hall Bench↑	Avg.↑
LLaVA-1.5-13B	1528.7	70.2	38.3	40.8	90.0	89.6	44.7	52.9	
+Ours	1547.6 <u>18.9</u>	71.1 <u>0.9</u>	40.5 <u>2.2</u>	39.1 <u>1.7</u>	92.4 <u>2.4</u>	92.7 <u>3.1</u>	47.2 <u>2.5</u>	55.3 <u>2.4</u>	↑ 3.6%
LLaVA-NeXT-13B	1583.5	68.8	42.3	36.0	91.9	92.4	48.2	54.3	
+Ours	1602.6 <u>19.1</u>	70.1 <u>1.3</u>	44.5 <u>2.2</u>	34.2 <u>1.8</u>	93.7 <u>1.8</u>	95.4 <u>3.0</u>	50.8 <u>2.6</u>	56.8 <u>2.5</u>	↑ 3.6%
LLaVA-NeXT-34B	1644.9	78.6	54.6	27.6	91.4	94.1	48.9	55.0	
+Ours	1670.8 <u>25.9</u>	80.9 <u>2.3</u>	57.0 <u>2.4</u>	25.4 <u>2.2</u>	93.6 <u>2.2</u>	96.3 <u>2.2</u>	52.4 <u>3.5</u>	57.8 <u>2.8</u>	↑ 4.4%
Qwen2.5-VL-32B	1886.1	87.4	69.8	24.4	92.5	94.0	52.1	56.9	
+Ours*	1906.2 <u>20.1</u>	89.2 <u>1.8</u>	71.9 <u>2.1</u>	22.3 <u>2.1</u>	94.0 <u>1.5</u>	96.7 <u>2.7</u>	55.1 <u>3.0</u>	60.1 <u>3.2</u>	↑ 4.1%

7B (Liu et al., 2024a), LLaVA-v1.6-7B, LLaVA-NeXT-7B (Liu et al., 2024b), LLaVA-OV-7B (Li et al., 2025a), Qwen2-VL-7B (Wang et al., 2024b), and Qwen2.5-VL-7B (Bai et al., 2025). We choose four common MAS structures, including linear (Hong et al., 2024), layered (Ishibashi & Nishimura, 2024), random (Qian et al., 2025), and circular (Qian et al., 2025) structures. As

378
379 Table 4: Results across four augmented visual
380 benchmarks on circular MAS structure, including
381 multi-image and video based scenarios.

Base Agent	MMIU↑	MuirBench↑	MVBench↑	Video-MME↑	Avg.↑
LLaVA-NeXT-7B	31.6	42.6	49.2	60.4	
+Ours	33.9 <small>↑2.3</small>	44.3 <small>↑1.7</small>	52.0 <small>↑2.8</small>	61.9 <small>↑1.5</small>	↑4.9
LLaVA-OV-7B	36.9	54.2	56.1	67.8	
+Ours*	39.6 <small>↑2.7</small>	55.5 <small>↑1.3</small>	58.3 <small>↑2.2</small>	68.8 <small>↑1.0</small>	↑3.8
Qwen2-VL-7B	45.5	62.8	69.8	70.6	
+Ours*	47.7 <small>↑2.2</small>	64.0 <small>↑1.2</small>	71.0 <small>↑1.2</small>	71.7 <small>↑1.1</small>	↑2.5
Qwen2.5-VL-7B	47.4	64.0	72.3	73.4	
+Ours*	49.3 <small>↑1.9</small>	65.0 <small>↑1.0</small>	73.6 <small>↑1.3</small>	74.0 <small>↑0.6</small>	↑2.0

Table 5: Evaluations of multi-agent hallucination snowballing with proposed *HS* metric.

MAS Structure	CHAIR↓	POPE↓	AMBER↓	MMHal-Bench↓	HallBench↓	Avg.↓
Linear	17.2	25.7	26.8	35.3	40.2	
	12.4 <small>↓4.8</small>	16.4 <small>↓9.3</small>	15.9 <small>↓10.9</small>	22.6 <small>↓12.7</small>	24.8 <small>↓15.4</small>	↓35.8%
Layered	12.7	21.5	20.5	31.6	36.4	
	10.6 <small>↓2.1</small>	13.9 <small>↓7.6</small>	13.1 <small>↓7.4</small>	19.5 <small>↓12.1</small>	21.3 <small>↓15.1</small>	↓33.6%
Circular	18.9	29.1	31.1	40.8	47.4	
	12.8 <small>↓6.1</small>	17.0 <small>↓12.1</small>	17.7 <small>↓13.4</small>	24.1 <small>↓16.7</small>	27.8 <small>↓19.6</small>	↓39.8%
Random	15.5	23.4	23.8	36.8	42.5	
	10.3 <small>↓5.2</small>	15.0 <small>↓8.4</small>	16.4 <small>↓7.4</small>	21.2 <small>↓15.6</small>	25.6 <small>↓16.9</small>	↓36.5%

Table 6: Comparison results of other SOTA methods and ours on LLaVA-NeXT-7B and circular MAS structure. *Orig.* represents the original evaluation metric, and *HS* is our proposed one.

	CHAIR		POPE		AMBER		MMHal-Bench		HallBench		Avg.
	<i>Orig.</i> ↓	<i>HS</i> ↓	<i>Orig.</i> ↑	<i>HS</i> ↓	<i>Orig.</i> ↑	<i>HS</i> ↓	<i>Orig.</i> ↑	<i>HS</i> ↓	<i>Orig.</i> ↑	<i>HS</i> ↓	
Baseline	43.0	18.9	91.0	29.1	89.4	31.1	47.9	40.8	53.1	47.4	
MemVR	43.8 <small>↑0.8</small>	20.6 <small>↑1.7</small>	90.5 <small>↓0.5</small>	31.2 <small>↑2.1</small>	88.9 <small>↓0.5</small>	34.4 <small>↑3.3</small>	44.8 <small>↓3.1</small>	58.6 <small>↑17.8</small>	49.2 <small>↓3.9</small>	57.6 <small>↑10.2</small>	<small>↓2.6% ↑18.4%</small>
VISTA	43.4 <small>↑0.4</small>	19.0 <small>↑0.1</small>	91.2 <small>↑0.2</small>	27.8 <small>↓1.3</small>	90.5 <small>↑1.1</small>	28.3 <small>↓2.8</small>	46.3 <small>↓1.6</small>	47.4 <small>↑6.6</small>	50.7 <small>↓2.4</small>	53.3 <small>↑5.9</small>	<small>↓1.1% ↑3.1%</small>
FarSight	42.1 <small>↓0.9</small>	17.7 <small>↓1.2</small>	91.9 <small>↑0.9</small>	22.7 <small>↓6.4</small>	91.0 <small>↑1.6</small>	26.6 <small>↓4.5</small>	47.4 <small>↓0.5</small>	42.9 <small>↑2.1</small>	51.9 <small>↓1.2</small>	52.4 <small>↑5.0</small>	<small>↓0.5% ↓5.4%</small>
DeCo	42.6 <small>↓0.4</small>	18.2 <small>↓0.7</small>	91.3 <small>↑0.3</small>	25.1 <small>↓4.0</small>	91.6 <small>↑2.2</small>	24.3 <small>↓6.8</small>	47.0 <small>↓0.9</small>	44.1 <small>↑3.3</small>	50.4 <small>↓2.7</small>	53.0 <small>↑5.6</small>	<small>↓1.0% ↓3.8%</small>
TAME	42.1 <small>↓0.9</small>	18.8 <small>↓0.1</small>	91.4 <small>↑0.4</small>	22.8 <small>↓6.3</small>	91.9 <small>↑2.5</small>	22.7 <small>↓8.4</small>	46.5 <small>↓1.4</small>	47.8 <small>↑7.0</small>	49.9 <small>↓3.2</small>	53.8 <small>↑6.4</small>	<small>↓1.6% ↓3.7%</small>
Ours	41.2 <small>↓1.8</small>	12.8 <small>↓6.1</small>	93.3 <small>↑2.3</small>	17.0 <small>↓12.1</small>	92.7 <small>↑3.3</small>	17.7 <small>↓13.4</small>	51.1 <small>↑3.2</small>	24.1 <small>↓16.7</small>	55.7 <small>↑2.6</small>	27.8 <small>↓19.6</small>	<small>↑3.8% ↓39.8%</small>

401 mentioned in Appendix C.1, we primarily follow the multi-agent collaboration strategy with linear
402 increased context length, allowing the scaling of MAS. As demonstrated in Table 2, our ViF
403 consistently enhances the average performance of the six baselines by 2.4-3.8%, verifying the
404 compatibility of our method on various MAS structures based on arbitrary base VLMs. Notably, on
405 the MMHal-Bench and HallBench benchmarks, which are more sophisticated and have unsatisfactory
406 baseline performance, our ViF achieves over 4% average improvement. When applied to the
407 circular structure, which is hallucination-concentrated with densest collaborations and interactions
408 among agents, our ViF dramatically reduces hallucination snowballing and further improves the
409 performance by 3% among the six base models, compared to the other three selected structures.

410 As reported in Table 3, we also analyze the performance of our proposed ViF on the scaled-up
411 models with higher parameters. It is observed that when equipped with our ViF, the larger base
412 models featuring more than 30B parameters, *e.g.*, LLaVA-NeXT-34B and Qwen-2.5-VL-32B, ex-
413 hibit greater enhancement than all smaller ones, improving by more than 4% across all benchmarks.
414 This indicates that our model-agnostic method effectively improves their comprehensive perfor-
415 mance, likely because larger-parameter baselines possess stronger fundamental capabilities, and our
416 approach specifically unlocks their latent potential in multi-agent scenarios.

417 **Performance on Augmented Visual Benchmarks.** We include additional four benchmarks of
418 two augmented visual domains, including two multi-image based benchmarks: MMIU, MuirBench;
419 video based two benchmarks: MVBench, Video-MME. As presented in Table 4, our ViF method ex-
420 hibits significant improvements relative to the base models across multi-image and video scenarios.
421 Specifically, it yields an average 2.0-4.9% performance improvement across the four base models
422 and four additional benchmarks, demonstrating robust performance in multiple visual scenarios.

423 **Multi-Agent Hallucination Snowballing Mitigation.** In addition to the results of original metrics,
424 we attempt to assess the level of hallucination snowballing in MAS quantitatively. Thus, we formally
425 define a hallucination snowballing score (*HS*) as in Equation 7, measuring both the hallucination
426 level and propagation in MAS. As reported in Table 5, adding our ViF reduces at least 30% *HS*
427 score on the average of five hallucination benchmarks, significantly mitigating the hallucination
428 propagation from the textual flow of visual contents. Notably, the layered structure suffers the
429 least from the detrimental snowballing, while in circular structure, where the initial hallucination
430 snowballing is the most serious, the reduction of the score from our method is almost 40%.

431 **Comparison Results.** We compare the results of another five model-agnostic and token-wise
432 hallucination mitigation methodologies in multi-agent contexts, *i.e.*, MemVR (Zou et al., 2025),

VISTA (Li et al., 2025c), FarSight (Tang et al., 2025b), DeCo (Wang et al., 2025), and TAME (Tang et al., 2025a). Specifically, we retain the multi-agent experimental settings unchanged and apply these methodologies to the base model. These counterparts restrict the deepening of intrinsic hallucinations in a single model to some extent, however, in multi-agent scenarios, the propagation of visual contents via textual flow still introduces a vision-to-text cognitive bias and fails to restrain the snowballing of multi-agent hallucinations commendably.

As shown in Table 6, our introduced ViF approach achieves distinctly superior performance among all the benchmarks on both their original metrics and our proposed *HS* score. It obtains at least 4.2% enhancements in original metrics and 34.4% in *HS* score on average, compared to other methods tailored for single model hallucination mitigation. Although these counterparts are impressively efficacious in single VLM, their performance is compromised when applied to MAS, because of the failure to deal with hallucination propagation among agents and further snowballing. Surprisingly, in MAS environments, the results of these counterparts are even inferior to the baseline, especially on challenging ones. This counterintuitive observation is likely because they modify the initial paradigm of decoding or attention in VLMs, but retain the textual flow to relay visual information, which amplifies the preference for text over vision tokens. Our method, adopting visual flow to relay information among agents, cuts the *HS* score almost in half and delivers tangible improvements in the mitigation of hallucination snowballing.

4.2 ADDITIONAL ANALYSES

Impact of the Number of Agent Turns. To achieve satisfactory completion, typically, MAS necessitates a greater number of agent turns in more complicated and challenging tasks. However, the hallucination snowballing effect restricts the multi-turn collaboration among agents, where hallucinations are amplified and propagated, leading to suboptimal performance. Therefore, we compare our ViF with baselines and other counterparts to assess the impact of the number of agent turns.

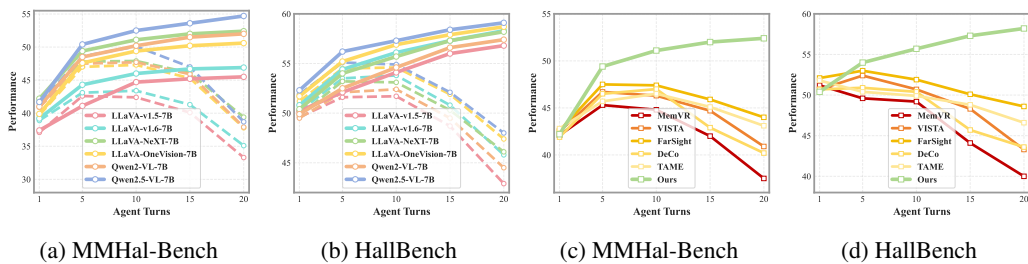


Figure 7: Impact of the number of agent turns. In (a) and (b), straight and dashed lines are the results with or without our ViF on various baselines and circular MAS structure, respectively. (c) and (d) show the results between other counterparts and our method based on LLaVA-NeXT-7B.

As demonstrated in Figure 7, our method maintains an upward trend in performance as the number of agent turns increases, while both other contrast methods and baselines experience performance degradation instead. More precisely, when the agent turn is set to one, which is equivalent to a single-agent context, ViF exhibits only a marginal improvement over the baselines, and falls behind some other methods designed for hallucination mitigation in a single model. As the turning trends of the baselines in Figure 7a and 7b show, the performance begins to deteriorate when the turns are only increased to 5, and at the 20th turn, their performance is even further less than that of a single agent. Further compare with other methods as illustrated in Figure 7c and 7d, although hallucinations are mitigated in early turns to some extent, the hallucination snowballing phenomenon still suffers in later turns, essentially limiting the multi-agent collaboration and inhibiting the potential of MAS.

Ablation and Sensitivity Analyses. To verify the effectiveness of each component in our ViF, we perform ablations on the visual relay tokens and the attention reallocation. As reported in Table 7, the improvement from visual flow to relay information is prominent, and the results are still better than most comparison methods even when ablating half of the visual relay tokens, showcasing excellent robustness. The reallocation mechanism further optimizes the attention distribution among different tokens and activates visual relay tokens, which is beneficial to our designs of visual relay flow.

486
 487 **Table 8: Efficiency comparison between our ViF and the base models on the circular MAS archi-**
 488 **ture. All base models are evaluated in the multi-agent environment to quantify the additional**
 489 **latency introduced by ViF, including the average *latency* (seconds), and the average floating point**
 490 **operations, *i.e.*, *FLOPs* (T).**

Base Agent	CHAIR		POPE		AMBER		MMHal-Bench		HallBench	
	Latency↓	FLOPs↓	Latency↓	FLOPs↓	Latency↓	FLOPs↓	Latency↓	FLOPs↓	Latency↓	FLOPs↓
LLaVA-NeXT-7B	3.16	157.3	2.46	103.4	2.79	127.2	3.48	184.0	3.91	248.3
+Ours	3.47	168.5	2.79	115.7	3.10	138.9	3.83	197.6	4.23	260.3
LLaVA-NeXT-13B	5.88	308.5	5.63	279.0	5.93	310.0	6.33	357.4	7.64	386.8
+Ours	6.17	320.6	5.91	289.6	6.25	321.2	6.67	372.8	8.03	399.6
LLaVA-NeXT-34B	8.80	417.2	8.49	387.3	8.61	408.7	9.41	444.1	11.06	478.1
+Ours	9.09	419.1	8.79	398.8	8.92	419.8	9.75	457.7	11.41	493.8

500 Furthermore, as listed in Table 12, 13,
 501 and 14, we conduct an analysis of
 502 the sensitivity of key hyper-parameters,
 503 *i.e.*, the salience threshold ω , the tem-
 504 perature scaling τ , and the reallocation
 505 coefficient α , quantitatively assess their
 506 impact on model performance, and de-
 507 termine a rational set of values.

508 **Efficiency.** To assess the inference effi-
 509 ciency, particularly in multi-agent con-
 510 texts, we first compare the time and
 511 computational overheads of our pro-
 512 posed ViF with those of the base mod-
 513 els. As reported in Table 8, our ViF exhibits high efficiency with moderate overheads, incurring an
 514 additional 8.1-13.4% inference latency and 4.8-11.9% computational costs (measured by *FLOPs*)
 515 over the base model across five selected benchmarks. These extra overheads mainly stem from the
 516 intrinsic components of ViF. Thus, the extra overhead remains stable across base models of varying
 517 scales and exhibits only slightly linear increase. Notably, the additional latency and computation are
 518 even more negligible for larger models, which are less than 4% and 3% on LLaVA-NeXT-34B. Fur-
 519 thermore, as presented in Table 15, the time and computational overhead of our ViF remain efficient
 520 when feeding visual images with varying resolutions and across different agent turns.

5 CONCLUSION

524 We unveil the phenomenon of multi-agent visual hallucination snowballing existing in MAS, where
 525 subsequent agents progressively amplify errors originating in a single agent through textual infor-
 526 mation flow that relays visual messages. Based on extensive analyses, the essence of hallucination
 527 snowballing lies in a subset of vision tokens with an unimodal attention peak, well-preserving the
 528 visual information, but these tokens gradually diminish with the increase in the agent turns. To al-
 529 leviate this problem, a model-agnostic method named ViF is proposed, which redefines the visual
 530 information flow in MAS. Specifically, we introduce a visual flow to relay visual messages based
 531 on the selected unimodal vision tokens and utilize attention reallocation to optimize this pattern.
 532 Comprehensive experiments indicate that this novel paradigm is effective, robust, and compatible,
 533 paving the way for more efficient inter-agent visual information relay and more sophisticated MAS.

6 REPRODUCIBILITY STATEMENT

535 We have already elaborated on all the models or algorithms proposed, experimental configurations,
 536 and benchmarks used in the experiments in the main body or appendix of this paper. Furthermore,
 537 the entire code used in this work has been released.

540 7 THE USE OF LARGE LANGUAGE MODELS
 541

542 We solely use large language models for polishing our writing, and we have conducted a careful
 543 check, taking full responsibility for all content in this work.
 544

545 REFERENCES
 546

547 Dosovitskiy Alexey. An image is worth 16x16 words: Transformers for image recognition at scale.
 548 *arXiv preprint arXiv: 2010.11929*, 2020.
 549

550 Wenbin An, Feng Tian, Sicong Leng, Jiahao Nie, Haonan Lin, QianYing Wang, Guang Dai, Ping
 551 Chen, and Shijian Lu. Agla: Mitigating object hallucinations in large vision-language models
 552 with assembly of global and local attention. *arXiv preprint arXiv:2406.12718*, 2024.

553 Shuai Bai, Keqin Chen, Xuejing Liu, Jialin Wang, Wenbin Ge, Sibo Song, Kai Dang, Peng Wang,
 554 Shijie Wang, Jun Tang, et al. Qwen2.5-vl technical report. *arXiv preprint arXiv:2502.13923*,
 555 2025.
 556

557 Mert Cemri, Melissa Z Pan, Shuyi Yang, Lakshya A Agrawal, Bhavya Chopra, Rishabh Tiwari, Kurt
 558 Keutzer, Aditya Parameswaran, Dan Klein, Kannan Ramchandran, et al. Why do multi-agent llm
 559 systems fail? *arXiv preprint arXiv:2503.13657*, 2025.

560 Zhanpeng Chen, Mingxiao Li, Ziyang Chen, Nan Du, Xiaolong Li, and Yuexian Zou. [Advancing general multimodal capability of vision-language models with pyramid-descent visual position encoding](#). *arXiv preprint arXiv:2501.10967*, 2025.
 561

562 Zhe Chen, Weiyun Wang, Yue Cao, Yangzhou Liu, Zhangwei Gao, Erfei Cui, Jinguo Zhu, Shen-
 563 glong Ye, Hao Tian, Zhaoyang Liu, et al. Expanding performance boundaries of open-source
 564 multimodal models with model, data, and test-time scaling. *arXiv preprint arXiv:2412.05271*,
 565 2024a.
 566

567 Zhe Chen, Jiannan Wu, Wenhui Wang, Weijie Su, Guo Chen, Sen Xing, Muyan Zhong, Qinglong
 568 Zhang, Xizhou Zhu, Lewei Lu, et al. Internvl: Scaling up vision foundation models and aligning
 569 for generic visual-linguistic tasks. In *Proceedings of the IEEE/CVF Conference on Computer*
 570 *Vision and Pattern Recognition (CVPR)*, pp. 24185–24198, 2024b.
 571

572 Gheorghe Comanici, Eric Bieber, Mike Schaeckermann, Ice Pasupat, Noveen Sachdeva, Inderjit
 573 Dhillon, Marcel Blstein, Ori Ram, Dan Zhang, Evan Rosen, et al. Gemini 2.5: Pushing the
 574 frontier with advanced reasoning, multimodality, long context, and next generation agentic capa-
 575 bilities. *arXiv preprint arXiv:2507.06261*, 2025.
 576

577 Tri Dao. Flashattention-2: Faster attention with better parallelism and work partitioning. In *The*
 578 *Twelfth International Conference on Learning Representations (ICLR)*, 2024.
 579

580 Timothée Darcet, Maxime Oquab, Julien Mairal, and Piotr Bojanowski. Vision transformers need
 581 registers. In *The Twelfth International Conference on Learning Representations (ICLR)*, 2024.
 582

583 Chaoyou Fu, Yuhang Dai, Yongdong Luo, Lei Li, Shuhuai Ren, Renrui Zhang, Zihan Wang, Chenyu
 584 Zhou, Yunhang Shen, Mengdan Zhang, et al. Video-mme: The first-ever comprehensive eval-
 585 uation benchmark of multi-modal llms in video analysis. In *Proceedings of the Computer Vision*
 586 *and Pattern Recognition Conference*, pp. 24108–24118, 2025.

587 Xuan Gong, Tianshi Ming, Xinpeng Wang, and Zhihua Wei. DAMRO: Dive into the attention
 588 mechanism of LVLM to reduce object hallucination. In *Proceedings of the 2024 Conference on*
 589 *Empirical Methods in Natural Language Processing (EMNLP)*, pp. 7696–7712, Miami, Florida,
 590 USA, November 2024. Association for Computational Linguistics.
 591

592 Aaron Grattafiori, Abhimanyu Dubey, Abhinav Jauhri, Abhinav Pandey, Abhishek Kadian, Ahmad
 593 Al-Dahle, Aiesha Letman, Akhil Mathur, Alan Schelten, Alex Vaughan, et al. The llama 3 herd
 594 of models. *arXiv preprint arXiv:2407.21783*, 2024.

594 Tianrui Guan, Fuxiao Liu, Xiyang Wu, Ruiqi Xian, Zongxia Li, Xiaoyu Liu, Xijun Wang, Lichang
 595 Chen, Furong Huang, Yaser Yacoob, et al. Hallusionbench: an advanced diagnostic suite for
 596 entangled language hallucination and visual illusion in large vision-language models. In *Pro-
 ceedings of the IEEE/CVF Conference on Computer Vision and Pattern Recognition (CVPR)*, pp.
 597 14375–14385, 2024.

599 Taicheng Guo, Xiuying Chen, Yaqi Wang, Ruidi Chang, Shichao Pei, Nitesh V Chawla, Olaf Wiest,
 600 and Xiangliang Zhang. Large language model based multi-agents: A survey of progress and
 601 challenges. *arXiv preprint arXiv:2402.01680*, 2024.

603 Sirui Hong, Mingchen Zhuge, Jonathan Chen, Xiawu Zheng, Yuheng Cheng, Jinlin Wang, Ceyao
 604 Zhang, Zili Wang, Steven Ka Shing Yau, Zijuan Lin, Liyang Zhou, Chenyu Ran, Lingfeng Xiao,
 605 Chenglin Wu, and Jürgen Schmidhuber. Metagpt: Meta programming for a multi-agent collabora-
 606 tive framework. In *The Twelfth International Conference on Learning Representations (ICLR)*,
 607 2024.

608 Shengding Hu, Yuge Tu, Xu Han, Ganqu Cui, Chaoqun He, Weilin Zhao, Xiang Long, Zhi Zheng,
 609 Yewei Fang, Yuxiang Huang, Xinrong Zhang, Zhen Leng Thai, Chongyi Wang, Yuan Yao,
 610 Chenyang Zhao, Jie Zhou, Jie Cai, Zhongwu Zhai, Ning Ding, Chao Jia, Guoyang Zeng, da-
 611 hai li, Zhiyuan Liu, and Maosong Sun. MiniCPM: Unveiling the potential of small language
 612 models with scalable training strategies. In *First Conference on Language Modeling (COLM)*,
 613 2024.

614 Qidong Huang, Xiaoyi Dong, Pan Zhang, Bin Wang, Conghui He, Jiaqi Wang, Dahua Lin, Weiming
 615 Zhang, and Nenghai Yu. [Opera: Alleviating hallucination in multi-modal large language models
 via over-trust penalty and retrospection-allocation](#). In *Proceedings of the IEEE/CVF Conference
 616 on Computer Vision and Pattern Recognition (CVPR)*, pp. 13418–13427, 2024.

617 Fushuo Huo, Wenchao Xu, Zhong Zhang, Haozhao Wang, Zhicheng Chen, and Peilin Zhao. Self-
 618 introspective decoding: Alleviating hallucinations for large vision-language models. In *The Thir-
 619 teenth International Conference on Learning Representations (ICLR)*, 2025.

620 Yoichi Ishibashi and Yoshimasa Nishimura. Self-organized agents: A llm multi-agent framework
 621 toward ultra large-scale code generation and optimization. *arXiv preprint arXiv:2404.02183*,
 622 2024.

623 Seongyun Lee, Sue Hyun Park, Yongrae Jo, and Minjoon Seo. Volcano: Mitigating multimodal
 624 hallucination through self-feedback guided revision. In *Proceedings of the 2024 Conference of
 625 the North American Chapter of the Association for Computational Linguistics: Human Language
 626 Technologies (ACL: Long Papers)*, pp. 391–404, Mexico City, Mexico, June 2024. Association
 627 for Computational Linguistics.

628 Bo Li, Yuanhan Zhang, Dong Guo, Renrui Zhang, Feng Li, Hao Zhang, Kaichen Zhang, Peiyuan
 629 Zhang, Yanwei Li, Ziwei Liu, and Chunyuan Li. Llava-onevision: Easy visual task transfer.
 630 *Transactions on Machine Learning Research (TMLR)*, 2025a. ISSN 2835-8856.

631 Kunchang Li, Yali Wang, Yinan He, Yizhuo Li, Yi Wang, Yi Liu, Zun Wang, Jilan Xu, Guo Chen,
 632 Ping Luo, et al. Mvbench: A comprehensive multi-modal video understanding benchmark. In
 633 *Proceedings of the IEEE/CVF Conference on Computer Vision and Pattern Recognition*, pp.
 634 22195–22206, 2024.

635 Yifan Li, Yifan Du, Kun Zhou, Jinpeng Wang, Xin Zhao, and Ji-Rong Wen. Evaluating object hal-
 636 lucination in large vision-language models. In *Proceedings of the 2023 Conference on Empirical
 637 Methods in Natural Language Processing (EMNLP)*, pp. 292–305, Singapore, December 2023.
 638 Association for Computational Linguistics.

639 Yubo Li, Xiaobin Shen, Xinyu Yao, Xueying Ding, Yidi Miao, Ramayya Krishnan, and Rema Pad-
 640 man. Beyond single-turn: A survey on multi-turn interactions with large language models. *arXiv
 641 preprint arXiv:2504.04717*, 2025b.

642 Zhuowei Li, Haizhou Shi, Yunhe Gao, Di Liu, Zhenting Wang, Yuxiao Chen, Ting Liu, Long Zhao,
 643 Hao Wang, and Dimitris N. Metaxas. The hidden life of tokens: Reducing hallucination of large
 644 vision-language models via visual information steering. In *The Forty-second International Con-
 645 ference on Machine Learning (ICML)*, 2025c.

648 Haotian Liu, Chunyuan Li, Yuheng Li, and Yong Jae Lee. Improved baselines with visual instruction
 649 tuning. In *Proceedings of the IEEE/CVF Conference on Computer Vision and Pattern Recognition*
 650 (*CVPR*), pp. 26296–26306, 2024a.

651

652 Haotian Liu, Chunyuan Li, Yuheng Li, Bo Li, Yuanhan Zhang, Sheng Shen, and Yong Jae Lee.
 653 Llava-next: Improved reasoning, ocr, and world knowledge, January 2024b. URL <https://llava-vl.github.io/blog/2024-01-30-llava-next/>.

654

655 Sheng Liu, Xu Zhang, Nitesh Sekhar, Yue Wu, Prateek Singhal, and Carlos Fernandez-Granda.
 656 Avoiding spurious correlations via logit correction. In *The Eleventh International Conference on*
 657 *Learning Representations (ICLR)*, 2023.

658

659 Shi Liu, Kecheng Zheng, and Wei Chen. Paying more attention to image: A training-free method
 660 for alleviating hallucination in lmlms. *arXiv preprint arXiv:2407.21771*, 2024c.

661

662 Yuan Liu, Haodong Duan, Yuanhan Zhang, Bo Li, Songyang Zhang, Wangbo Zhao, Yike Yuan,
 663 Jiaqi Wang, Conghui He, Ziwei Liu, et al. Mmbench: Is your multi-modal model an all-around
 664 player? In *European Conference on Computer Vision (ECCV)*, pp. 216–233. Springer, 2024d.

665

666 Ilya Loshchilov and Frank Hutter. Decoupled weight decay regularization. In *International Confer-
 667 ence on Learning Representations (ICLR)*, 2019.

668

669 Shiyin Lu, Yang Li, Qing-Guo Chen, Zhao Xu, Weihua Luo, Kaifu Zhang, and Han-Jia Ye.
 670 Ovis: Structural embedding alignment for multimodal large language model. *arXiv preprint*
 671 *arXiv:2405.20797*, 2024.

672

673 Shiyin Lu, Yang Li, Yu Xia, Yuwei Hu, Shanshan Zhao, Yanqing Ma, Zhichao Wei, Yinglun Li,
 674 Lunhao Duan, Jianshan Zhao, et al. Ovis2. 5 technical report. *arXiv preprint arXiv:2508.11737*,
 675 2025.

676

677 Sachin Mehta, Marjan Ghazvininejad, Srinivasan Iyer, Luke Zettlemoyer, and Hannaneh Hajishirzi.
 678 Delight: Deep and light-weight transformer. In *International Conference on Learning Represen-
 679 tations (ICLR)*, 2021.

680

681 Fanqing Meng, Jin Wang, Chuanhao Li, Quanfeng Lu, Hao Tian, Jiaqi Liao, Xizhou Zhu, Jifeng
 682 Dai, Yu Qiao, Ping Luo, et al. Mmiu: Multimodal multi-image understanding for evaluating large
 683 vision-language models. *arXiv preprint arXiv:2408.02718*, 2024.

684

685 Clement Neo, Luke Ong, Philip Torr, Mor Geva, David Krueger, and Fazl Barez. Towards inter-
 686 preting visual information processing in vision-language models. In *The Thirteenth International*
 687 *Conference on Learning Representations (ICLR)*, 2025.

688

689 Chen Qian, Zihao Xie, YiFei Wang, Wei Liu, Kunlun Zhu, Hanchen Xia, Yufan Dang, Zhuoyun Du,
 690 Weize Chen, Cheng Yang, Zhiyuan Liu, and Maosong Sun. Scaling large language model-based
 691 multi-agent collaboration. In *The Thirteenth International Conference on Learning Representa-
 692 tions (ICLR)*, 2025.

693

694 Anna Rohrbach, Lisa Anne Hendricks, Kaylee Burns, Trevor Darrell, and Kate Saenko. Object hal-
 695 lucination in image captioning. In *Proceedings of the 2018 Conference on Empirical Methods in*
 696 *Natural Language Processing (EMNLP)*, pp. 4035–4045, Brussels, Belgium, October–November
 697 2018. Association for Computational Linguistics.

698

699 Oscar Skean, Md Rifat Arefin, Dan Zhao, Niket Nikul Patel, Jalal Naghiyev, Yann LeCun, and
 700 Ravid Shwartz-Ziv. Layer by layer: Uncovering hidden representations in language models. In
 701 *Forty-second International Conference on Machine Learning (ICML)*, 2025.

702

703 Zhiqing Sun, Sheng Shen, Shengcao Cao, Haotian Liu, Chunyuan Li, Yikang Shen, Chuang Gan,
 704 Liang-Yan Gui, Yu-Xiong Wang, Yiming Yang, et al. Aligning large multimodal models with
 705 factually augmented rlhf. *arXiv preprint arXiv:2309.14525*, 2023.

706

707 Feilong Tang, Zile Huang, Chengzhi Liu, Qiang Sun, Harry Yang, and Ser-Nam Lim. Intervening
 708 anchor token: Decoding strategy in alleviating hallucinations for MLLMs. In *The Thirteenth*
 709 *International Conference on Learning Representations (ICLR)*, 2025a.

702 Feilong Tang, Chengzhi Liu, Zhongxing Xu, Ming Hu, Zile Huang, Haochen Xue, Ziyang Chen,
 703 Zelin Peng, Zhiwei Yang, Sijin Zhou, et al. Seeing far and clearly: Mitigating hallucinations
 704 in mllms with attention causal decoding. In *Proceedings of the Computer Vision and Pattern
 705 Recognition Conference (CVPR)*, pp. 26147–26159, 2025b.

706 707 Qwen Team. Qwen2 technical report. *arXiv preprint arXiv:2407.10671*, 2024.

708 709 Chenxi Wang, Xiang Chen, Ningyu Zhang, Bozhong Tian, Haoming Xu, Shumin Deng, and Huajun
 710 Chen. Mllm can see? dynamic correction decoding for hallucination mitigation. In *The Thirteenth
 711 International Conference on Learning Representations (ICLR)*, 2025.

712 713 Fei Wang, Xingyu Fu, James Y Huang, Zekun Li, Qin Liu, Xiaogeng Liu, Mingyu Derek Ma,
 714 Nan Xu, Wenxuan Zhou, Kai Zhang, et al. Muirbench: A comprehensive benchmark for robust
 715 multi-image understanding. *arXiv preprint arXiv:2406.09411*, 2024a.

716 717 Junyang Wang, Yuhang Wang, Guohai Xu, Jing Zhang, Yukai Gu, Haitao Jia, Jiaqi Wang, Haiyang
 718 Xu, Ming Yan, Ji Zhang, et al. Amber: An llm-free multi-dimensional benchmark for mllms
 719 hallucination evaluation. *arXiv preprint arXiv:2311.07397*, 2023.

720 721 Peng Wang, Shuai Bai, Sinan Tan, Shijie Wang, Zhihao Fan, Jinze Bai, Keqin Chen, Xuejing Liu,
 722 Jialin Wang, Wenbin Ge, et al. Qwen2-vl: Enhancing vision-language model’s perception of the
 723 world at any resolution. *arXiv preprint arXiv:2409.12191*, 2024b.

724 725 Xintong Wang, Jingheng Pan, Liang Ding, and Chris Biemann. Mitigating hallucinations in large
 726 vision-language models with instruction contrastive decoding. In *Findings of the Association
 727 for Computational Linguistics: ACL 2024*, pp. 15840–15853, Bangkok, Thailand, August 2024c.
 728 Association for Computational Linguistics.

729 730 Zichen Wen, Yifeng Gao, Shaobo Wang, Junyuan Zhang, Qintong Zhang, Weijia Li, Conghui He,
 731 and Linfeng Zhang. Stop looking for important tokens in multimodal language models: Duplication
 732 matters more. *arXiv preprint arXiv:2502.11494*, 2025.

733 734 Dingchen Yang, Bowen Cao, Guang Chen, and Changjun Jiang. Pensieve: Retrospect-then-compare
 735 mitigates visual hallucination. *arXiv preprint arXiv:2403.14401*, 2024.

736 737 Hao Yin, Guangzong Si, and Zilei Wang. Clearsight: Visual signal enhancement for object hallucination
 738 mitigation in multimodal large language models. In *Proceedings of the Computer Vision and Pattern
 739 Recognition Conference (CVPR)*, pp. 14625–14634, 2025.

740 741 Shukang Yin, Chaoyou Fu, Sirui Zhao, Tong Xu, Hao Wang, Dianbo Sui, Yunhang Shen, Ke Li,
 742 Xing Sun, and Enhong Chen. Woodpecker: Hallucination correction for multimodal large
 743 language models. *arXiv preprint arXiv:2310.16045*, 2023.

744 745 Shukang Yin, Chaoyou Fu, Sirui Zhao, Ke Li, Xing Sun, Tong Xu, and Enhong Chen. A survey on
 746 multimodal large language models. *National Science Review*, 11(12):nwae403, 2024.

747 748 Weihao Yu, Zhengyuan Yang, Linjie Li, Jianfeng Wang, Kevin Lin, Zicheng Liu, Xinchao Wang,
 749 and Lijuan Wang. Mm-vet: Evaluating large multimodal models for integrated capabilities. In
 750 *The Forty-first International Conference on Machine Learning (ICML)*, 2024.

751 752 Xinlei Yu, Zhangquan Chen, Yudong Zhang, Shilin Lu, Ruolin Shen, Jiangning Zhang, Xiaobin
 753 Hu, Yanwei Fu, and Shuicheng Yan. Visual document understanding and question answering:
 754 A multi-agent collaboration framework with test-time scaling. *arXiv preprint arXiv:2508.03404*,
 755 2025.

756 757 Zihao Yue, Liang Zhang, and Qin Jin. Less is more: Mitigating multimodal hallucination from
 758 an eos decision perspective. In *Proceedings of the 62nd Annual Meeting of the Association for
 759 Computational Linguistics (ACL: Long Papers)*, pp. 11766–11781, Bangkok, Thailand, August
 760 2024. Association for Computational Linguistics.

761 762 Bohan Zhai, Shijia Yang, Xiangchen Zhao, Chenfeng Xu, Sheng Shen, Dongdi Zhao, Kurt Keutzer,
 763 Manling Li, Tan Yan, and Xiangjun Fan. Halle-switch: Rethinking and controlling object
 764 existence hallucinations in large vision language models for detailed caption. *arXiv preprint
 765 arXiv:2310.01779*, 2023.

756 Guibin Zhang, Yanwei Yue, Xiangguo Sun, Guancheng Wan, Miao Yu, Junfeng Fang, Kun Wang,
 757 Tianlong Chen, and Dawei Cheng. G-designer: Architecting multi-agent communication topolo-
 758 gies via graph neural networks. *arXiv preprint arXiv:2410.11782*, 2024a.

759
 760 Guibin Zhang, Luyang Niu, Junfeng Fang, Kun Wang, LEI BAI, and Xiang Wang. Multi-agent
 761 architecture search via agentic supernet. In *Forty-second International Conference on Machine
 762 Learning (ICLR)*, 2025a.

763 Muru Zhang, Ofir Press, William Merrill, Alisa Liu, and Noah A. Smith. How language model
 764 hallucinations can snowball. In *The Forty-first International Conference on Machine Learning
 765 (ICML)*, 2024b.

766 Shaolei Zhang, Qingkai Fang, Zhe Yang, and Yang Feng. Llava-mini: Efficient image and video
 767 large multimodal models with one vision token. In *The Thirteenth International Conference on
 768 Learning Representations (ICLR)*, 2025b.

769
 770 Zhi Zhang, Srishti Yadav, Fengze Han, and Ekaterina Shutova. Cross-modal information flow in
 771 multimodal large language models. In *Proceedings of the Computer Vision and Pattern Recog-
 772 nition Conference (CVPR)*, pp. 19781–19791, 2025c.

773
 774 Weihong Zhong, Xiaocheng Feng, Liang Zhao, Qiming Li, Lei Huang, Yuxuan Gu, Weitao Ma,
 775 Yuan Xu, and Bing Qin. Investigating and mitigating the multimodal hallucination snowballing
 776 in large vision-language models. In *Proceedings of the 62nd Annual Meeting of the Association
 777 for Computational Linguistics (ACL: Long Papers)*, pp. 11991–12011. Association for Computa-
 778 tional Linguistics, August 2024.

779
 780 Yiyang Zhou, Chenhang Cui, Jaehong Yoon, Linjun Zhang, Zhun Deng, Chelsea Finn, Mohit
 781 Bansal, and Huaxiu Yao. Analyzing and mitigating object hallucination in large vision-language
 782 models. In *The Twelfth International Conference on Learning Representations (ICLR)*, 2024.

783
 784 Jinguo Zhu, Weiyun Wang, Zhe Chen, Zhaoyang Liu, Shenglong Ye, Lixin Gu, Hao Tian, Yuchen
 785 Duan, Weijie Su, Jie Shao, et al. Internvl3: Exploring advanced training and test-time recipes for
 786 open-source multimodal models. *arXiv preprint arXiv:2504.10479*, 2025.

787
 788 Xin Zou, Yizhou Wang, Yibo Yan, Yuanhuiyi Lyu, Kening Zheng, Sirui Huang, Junkai Chen, Peijie
 789 Jiang, Jia Liu, Chang Tang, and Xuming Hu. Look twice before you answer: Memory-space
 790 visual retracing for hallucination mitigation in multimodal large language models. *The Forty-
 791 second International Conference on Machine Learning (ICML)*, 2025.

792 APPENDIX

793 A RELATED WORKS

794
 795 **Visual Hallucination.** The tendency of VLMs to generate plausible but non-factual or unsupported
 796 content, *i.e.*, visual hallucination, is well-documented in previous works. A common remedy has
 797 been to retrain or fine-tune models to better align outputs with ground truth (Zhou et al., 2024;
 798 Zhai et al., 2023; Yue et al., 2024), but these solutions often demand extensive training resources
 799 and additional data. Consequently, interest has grown in training-free techniques, including self-
 800 feedback correction (Lee et al., 2024; Yin et al., 2023), leveraging auxiliary models for external
 801 knowledge integration (Yang et al., 2024), and modifying decoding procedures (Wang et al., 2024c;
 802 Zou et al., 2025; Wang et al., 2025; Tang et al., 2025b; Li et al., 2025c; Tang et al., 2025a; Yin
 803 et al., 2025; Liu et al., 2023). In contrast to these papers that focus on a single VLM agent, it is
 804 not sufficient to address the failure mode of hallucination snowballing that emerges in multi-agent
 805 collaboration, which is the core focus of our paper.

806
 807 **Attention in VLM-Based Agents.** The hallucination problem of VLMs can be mainly attributed to
 808 and indicated by the attention mechanism. Earlier work found that LVLMs tend to attend to broad,
 809 global image cues and miss prompt-relevant details (Dariset et al., 2024; Gong et al., 2024; An et al.,
 810 2024), a behavior often traced to the Vision Transformer encoder (Alexey, 2020). To address this,
 811 some methods boost attention weights for pertinent image tokens (Liu et al., 2024c), others select

810 or filter informative visual features and apply contrastive decoding to suppress hallucinations (Huo
 811 et al., 2025). Our work presents an extensive study on the attention allocation token and layer-wise
 812 analysis to provide a better understanding of how multi-agent pipelines lose visual fidelity during
 813 inference turns. Based on this, we further introduce a novel visual flow to alleviate hallucination
 814 snowballing in multi-agent systems.

817 B REQUISITE ANALYSES

819 B.1 SETTINGS

821 **Attention Allocation.** In Section 2, we first calculate the attention allocations of four tokens in
 822 different layers among different agent turns. Formally, we first denote the whole token set as \mathcal{T} ,
 823 consisting of vision token subset \mathcal{V} , instruction token subset \mathcal{I} , system token subset \mathcal{S} , and output
 824 token subset \mathcal{O} . The attention matrix is obtained as Equation 2, and each attention score $s_{i,j}$ indicates
 825 the attention from the i th token to the j th token. Thus, the attention allocation of a specific token
 826 type should be the sum of the attention score where the target is this token, which could be calculated
 827 as follows:

$$828 \quad Allocation_{token_type} = \sum_{i \in \mathcal{T}} \sum_{j \in \mathcal{T}} \mathcal{A}_l(i, j) \circ M_{token_type} = \sum_{i \in \mathcal{T}} \sum_{j \in \mathcal{T}} s_{i,j}, \quad (5)$$

$$832 \quad M_{token_type} = \mathbb{I}(i \in \mathcal{T}, j \in \mathcal{T}_{token_type}) \quad (6)$$

834 where \mathcal{A} denotes the average attention matrix in all attention heads of the l th layer in this context.
 835 The attention allocation of specific tokens explicitly represents the focus in each layer of the model
 836 when understanding the task and outputting the responses.

837 **Dropping Tokens in Certain Layers.** To drop subsets of vision tokens in shallow, middle, or
 838 deep layers, we set the hidden states of the subset in specific layers to zero instead of physical
 839 removal, because the latter changes sequence length and disrupts sequence alignment of the attention
 840 mechanism. Moreover, the implementation is mainly modified from (Liu et al., 2024b).

842 **Token Selection.** As described in Section 2, we select five subsets of vision tokens, and here we
 843 elaborate on the selection rules for each subset: (1) Random Tokens: we randomly select from all
 844 vision tokens, and limit the number of tokens in the subset to the average number in the other four
 845 subsets. Besides, we re-select the random tokens if the size of the largest connected component of
 846 selected tokens exceeds 10% of the total selected tokens, to avoid selecting centralized tokens that
 847 destroy randomness; (2) Inactive Tokens: we first calculate the average attention value across all layers
 848 for each token, then select tokens whose attention values are below the lower quartile and whose
 849 fluctuation does not exceed 20%; (3) Rise Tokens and (4) Fall Tokens: we select the tokens with
 850 gradually upward or downward attention allocation in the consecutive layers. To filter out insignifi-
 851 cant fluctuations and better reflect the overall attention trend of each token, we utilize a tolerance
 852 threshold. When deviations from the trend in the opposite direction do not exceed this threshold,
 853 we still consider it as maintaining the original trend; (5) Unimodal Tokens: we select tokens with
 854 attention allocation of a unimodal distribution, whose peak surpasses the salience threshold ω .

855 B.2 ADDITIONAL RESULTS

857 As discussed in Section 2, we use the results of the LLaVA-NeXT-7B (Liu et al., 2024b) model on
 858 POPE (Li et al., 2023) as an example. Here, we provide results of different base VLMs to verify
 859 the generality of our insights and to avoid model-specific conclusions. The token-wise attention
 860 allocations of vision, instruction, system, and output tokens of six common VLMs are demonstrated
 861 in Figure 13; the results of dropping different subsets of vision tokens in the shallow, middle and
 862 deep layers are listed in Table 16; and the proportion of different vision tokens among different agent
 863 turns are demonstrated in Figure 14. These experimental results from the six models are consistent
 864 with the previous conclusions, demonstrating excellent generalization across various models.

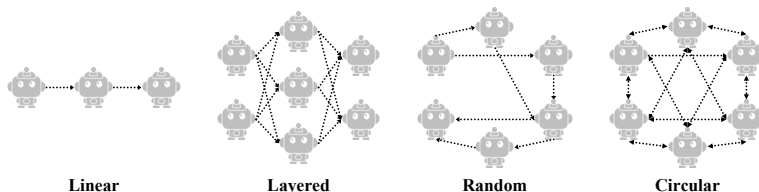


Figure 8: The four structures of MAS in our experiments.

C METHODOLOGIES

C.1 MAS STRUCTURES

Since our proposed ViF primarily centers on the snowballing of visual hallucinations in multi-agent contexts, we first briefly delineate the MAS structures defined herein. Existing MAS can be primarily categorized into two basic architectures (Guo et al., 2024): the centralized and the decentralized. The former are function-specialized, involving intricate collaborative workflows or functional division mechanisms. To mitigate such uncertainty, we adopt the latter decentralized ones, specifically incorporating four distributed structures that feature no central agent and a relatively straightforward structure; all agents are equal in status, save for sequential dependencies within the system. As illustrated in Figure 8, we include four particular sub-structures: linear structure (Hong et al., 2024), which implements a linear configuration for agent-mediated interactions; layered structure (Ishibashi & Nishimura, 2024), which comprises multiple hierarchical layers, where agent nodes within the current layer establish connections exclusively with those in the subsequent layer; random structure (Qian et al., 2025), which establishes random connections among agent nodes, where each agent may dynamically decide to redirect to the subsequent node based on current contextual information. Notably, this structure features unidirectional paths, thereby failing to ensure that a single node can reach all other nodes within the network; and circular structure (Qian et al., 2025), which utilizes fully-connected mesh, ensuring that each agent node can reach any other node in the system via at least one path. Intuitively, among the four MAS structures, circular ones have the densest collaborations and interactions among agents, and theoretically, the multi-agent hallucination snowballing effects are the most serious. Thus, all the experiments except the main results are conducted on the circular structure with more obvious visual hallucination snowballing.

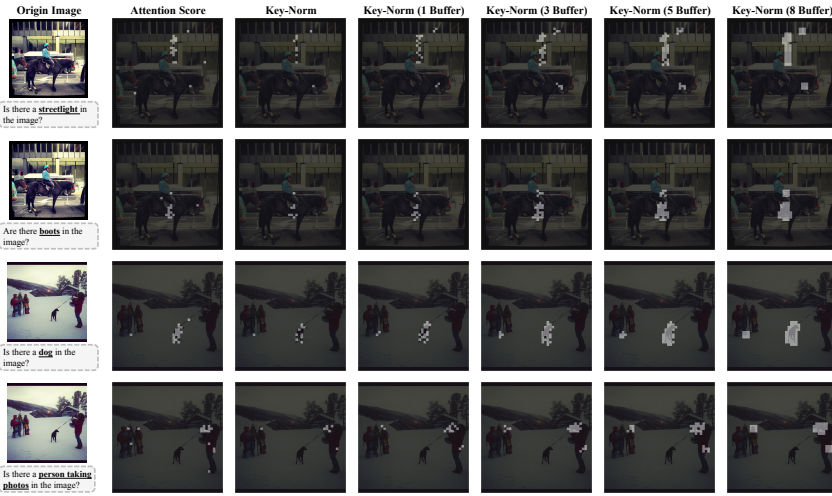
Primarily drawing on the multi-agent collaboration framework (Qian et al., 2025), we adopt an interactive collaboration strategy in our MAS, one anchored in topological ordering of directed acyclic graphs. This strategy employs a dual-agent multi-round interaction model: within each edge of the network, in the iterative interaction, adjacent actors are assigned to nodes, and critics are assigned to edges. Specifically, the preceding actor first requests feedback; the critic then provides reflective suggestions and requests further refinement; and finally, the subsequent actor generates an optimized artifact. Through this process, the prior artifact is iteratively refined. Specifically, this collaboration expand the conventional single agent method to multi-agent environments and reduces the context length from quadratic growth to linear growth, allowing the collaborative scaling law in MAS. Consequently, this architectural design is adopted as the core MAS framework in this work.

C.2 ALTERNATIVE OF ATTENTION SCORE BASED STRATEGY

Given that Flash-Attention 2/3 (Dao, 2024) are widely used in the latest VLMs, resulting in attention scores that are not explicitly stored and are not accessible, we design an alternative token selection strategy inspired by (Wen et al., 2025). Specifically, we utilize the L_2 norm of the key to replace the attention score, which reflects the feature strength of the token; a higher value of the norm indicates that the token is relatively more prominent and has more significant semantics. Unlike the strategy introduced in (Wen et al., 2025), which adopts L_1 norm, we choose L_2 norm to amplify the difference between tokens and promote the token selection. Statistically, the overlap of the initially selected tokens of the two strategies is more than 70%; however, the total amount of the Key-Norm based strategy is less than that of the other. Thus, we add buffer tokens of initially selected tokens, which surround the initially selected token of the 3×3 space.

918
919
920
Table 9: Results of the attention score based and other alternative strategies on LLaVA-NeXT-7B
921 and circular MAS structure.

Selection Strategy	MME↑	MM Bench↑	MM-Vet↑	CHAIR↓	POPE↑	AMBER↑	MMHal-Bench↑	Hall Bench↑
Value-Norm	1585.6 (-13.9)	72.3 (-2.3)	49.7 (-2.1)	43.4 (+2.2)	90.5 (-2.8)	90.1 (-2.6)	49.0 (-2.1)	53.6 (-2.1)
Value-Norm (+1 Buffer)	1587.4 (-12.1)	72.6 (-2.0)	49.9 (-1.9)	43.6 (+2.4)	90.6 (-2.7)	90.4 (-2.3)	49.4 (-1.7)	53.9 (-1.8)
Value-Norm (+3 Buffer)	1588.9 (-10.6)	72.7 (-1.9)	50.3 (-1.5)	43.1 (+1.9)	90.8 (-2.5)	90.3 (-2.4)	49.2 (-1.9)	53.9 (-1.8)
Value-Norm (+5 Buffer)	1590.2 (-9.3)	73.4 (-1.2)	50.5 (-1.3)	43.0 (+1.8)	91.1 (-2.2)	90.6 (-2.1)	49.4 (-1.7)	54.1 (-1.6)
Value-Norm (+8 Buffer)	1589.8 (-9.7)	73.3 (-1.3)	50.7 (-1.1)	43.3 (+2.1)	90.9 (-2.4)	90.8 (-1.9)	49.6 (-1.5)	54.4 (-1.3)
Key-Norm	1593.0 (-6.5)	74.0 (-0.6)	51.6 (-0.2)	41.5 (+0.3)	92.9 (-0.4)	92.1 (-0.6)	50.6 (-0.5)	55.1 (-0.6)
Key-Norm (+1 Buffer)	1594.4 (-5.1)	74.2 (-0.4)	51.7 (-0.1)	41.3 (+0.1)	93.1 (-0.2)	92.4 (-0.3)	50.9 (-0.2)	55.4 (-0.3)
Key-Norm (+3 Buffer)	1595.9 (-3.6)	74.3 (-0.3)	51.9 (+0.1)	41.2 (-0.0)	93.1 (-0.2)	92.6 (-0.1)	51.2 (+0.1)	55.5 (-0.2)
Key-Norm (+5 Buffer)	1595.2 (-4.3)	74.3 (-0.3)	51.7 (-0.1)	41.4 (+0.2)	92.8 (-0.5)	92.3 (-0.4)	50.9 (-0.2)	55.6 (-0.1)
Key-Norm (+8 Buffer)	1594.7 (-4.8)	74.4 (-0.2)	51.5 (-0.3)	41.6 (+0.4)	92.9 (-0.4)	92.3 (-0.4)	50.8 (-0.3)	55.4 (-0.3)
Attention Score	1599.5	74.6	51.8	41.2	93.3	92.7	51.1	55.7

918
919
920
Figure 9: Comparisons of selected tokens using the attention scores and other alternative strategies.

921
922
923
924
925
926
927
928
929
930
931
932
933
934
935
936
937
938
939
940
941
942
943
944
945
946
947
948
949
950
951
952
953
954
955
956
957
958
959
960
961
962
963
964
965
966
967
968
969
970
971
To verify the effectiveness of the Key-Norm, we compare it with the attention score based strategy as well as Value-Norm, which is similar to our alternative. As illustrated in Table 9, we observe that the Key-Norm based strategies are superior to the Value-Norm based ones. Besides, selecting by Key-Norm with three buffer tokens almost achieves the same performance as attention scores, even surpassing them in partial benchmarks. For more intuitive results, we provide the visualization comparisons of selected tokens based on these strategies from real cases. As visualized in Figure 9, the initial Key-Norm based selection covers the most visual relay tokens compared to the attention score based selection; however, the former one is relatively more sparse, losing partially important visual semantics. Adding buffer tokens is a good solution, which selects the surrounding tokens and supplements the information of the visual flow. It is worth noting that we add three buffer tokens when using the alternative strategy in our experiments, thereby balancing accuracy and efficiency.

963
964

D EXPERIMENTS

965
966

D.1 SETTINGS

967
968
Baselines. To verify the generality, we totally adopt ten models covering from 7B to 34B in our experiments, which are listed as follows:

969
970
971

- LLaVA-v1.5 (Liu et al., 2024a) uses a two-layer MLP to connect image features into the word embedding space, and we choose the 7B and 13B models, which have 32 and 40 layers in the decoder of the LLM, respectively.

- LLaVA-v1.6 (Liu et al., 2024b) increases resolution limits for input images with augmented data. It is the early version of LLaVA-NeXT, which has 32 layers in the LLM.
- LLaVA-NeXT (Liu et al., 2024b) has significant improvements in reasoning, OCR, and world knowledge, remaining the same structure as LLaVA-v1.6. We include 7B, 13B, and 34B models in our experiments, which have 32, 40, and 60 layers in the decoder.
- LLaVA-OV (Li et al., 2025a) is the most powerful base VLM in the LLaVA family, supporting single-image-, multi-image, and video scenes simultaneously. It uses the Qwen2 (Team, 2024) as the LLM, which has 28 layers.
- Qwen2-VL (Wang et al., 2024b) introduces naive dynamic resolution and multi-modal rotary position embedding (M-RoPE), achieving impressive image and video understanding. Its 7B model has 28 decoder layers.
- Qwen2.5-VL (Bai et al., 2025) compresses the vision tokens with an MLP-based fuser, aligns M-RoPE and absolute time, and meticulously designs a three-stage training pipeline. We select the 7B and 32B models with 32 layers of the LLM.

Benchmarks. We evaluate our method on eight widely adopted benchmarks, including three comprehensive benchmarks and five hallucination benchmarks, which are presented as follows:

- MME (Yin et al., 2024) is the first comprehensive benchmark and measures the perception and cognitive abilities of 14 challenging subtasks. Moreover, the metric is the total score across all the subtasks.
- MMBench (Liu et al., 2024d) consists of multiple-choice questions to assess over twenty different ability dimensions, offering a hierarchical framework with three levels. During the assessment, GPT-4 serves as the final judge. In our experiments, we only include the English subset for evaluation.
- MM-Vet (Yu et al., 2024) is a comprehensive benchmark, which defines six core capacities and assesses them on complicated visual tasks. It provides a GPT-4 based evaluator for open-ended outputs.
- CHAIR (Rohrbach et al., 2018) is a captioning hallucination assessment benchmark, comparing the objects mentioned in the title with the objects actually existing in the image. Here, we utilize the $CHAIR_S$ metric, calculating the proportion of titles that contain at least one hallucinatory object.
- POPE (Li et al., 2023) merges several classic visual datasets, and generates binary questions of the existence of objects. Each image is paired with six questions, and we use the accuracy metric.
- AMBER (Wang et al., 2023) is tailored to assess both generative and discriminative tasks, including existence, attribute, and relation hallucination. We follow the $AMBER$ score in the original paper.
- MMHal-Bench (Sun et al., 2023) is composed of high-quality image-question pairs to measure the hallucination, and the generated responses are automatically rated by GPT-4.
- HallBench (Guan et al., 2024) is meticulously handcrafted by experienced human experts, and evaluated by a text-only GPT4-assisted evaluation framework.
- MMIU (Meng et al., 2024) is designed to assess abilities across diverse multi-image tasks, encompassing 7 types of multi-image relationships, and 11K meticulously curated multiple-choice questions.
- MuirBench (Wang et al., 2024a) consists of 12 diverse multi-image tasks, utilizing a pairwise construction approach. Each standard instance is paired with a minimally semantically distinct unanswerable variant to ensure reliable assessment.
- MV-Bench (Li et al., 2024) covers 20 challenging video tasks intractable via single frames. Specifically, it transforms diverse static tasks into dynamic ones enables video tasks requiring a broad spectrum of temporal skills.
- Video-MME (Liu et al., 2024d) is the first full-spectrum benchmark in video analysis, distinguished by diverse video coverage, comprehensive temporal scope, multi-modal integration, and expert manual annotations, ensuring precise, reliable model assessment.

1026 Table 10: Two-stage training details. VLMs utilize various strategies to project vision tokens, such
 1027 as MLP-based projectors.

		Stage One Pre-Training	Stage Two Instruction Tuning
Modules	Vision Encoder	Frozen	Frozen
	Projector	Trainable	Trainable
	Large Language Model	Frozen	Trainable
	Transformer Block (Ours)	Trainable	Trainable
Settings	Batch Size	256	256
	Learning Rate	-	1e-4
	MM Learning Rate	5e-4	1e-5
	Warmup Ratio	0.05	0.02
	Optimizer	AdamW (Loshchilov & Hutter, 2019)	AdamW (Loshchilov & Hutter, 2019)
	Epoch	1	2

1039
 1040 **Evaluations.** For the eight selected benchmarks, we largely follow their original evaluation met-
 1041 rics. Besides, to assess the level of hallucination snowballing in multi-agent contexts, we propose a
 1042 hallucination snowballing score (HS), which quantifies both the severity and propagation of halluci-
 1043 nations. The score could be formulated as follows:

$$HS = \frac{1}{N} \sum_{i=1}^N \frac{1}{1 + \exp(\frac{D}{2} - d_i)} h_i, \quad (7)$$

1044 where d is the hallucination propagation distance, D and N are the total distance and the number of
 1045 agents in the multi-agent system. h represents the severity of hallucination, a centesimal-point scale
 1046 score produced by a judge model. Here, we employ GPT-5-20250807 as the judge with the prompt
 1047 as shown in the end of this paper. The average score on benchmarks measures the hallucination
 1048 snowballing; the deeper and broader the snowballing of the hallucination, the higher the score.

1049 To investigate the sensitivity of hallucination severity assessment, based on external judges, we con-
 1050 duct comparative experiments employing Gemini 2.5 Pro (Comanici et al., 2025) as the judge based
 1051 on POPE benchmark. We observe that over 94% of data discrepancies fall below 10%, demon-
 1052 strating the robustness of judge strategy. In practical applications, it suffices to ensure all comparisons
 1053 are conducted under identical judge settings to guarantee the fairness of evaluations.

1054 **Implementations.** Experiments are conducted on four or eight NVIDIA H20 96G GPUs. The
 1055 salience of unimodal morphology ω is 0.3, the temperature scaling τ is 0.8, the reallocation coeffi-
 1056 cient α_1, α_2 in the middle and deep layers are set to 0.1 and 0.3, and the temperature of generation
 1057 is set to 1 for MAS. For other configurations of baselines, we refer to the original paper.

1058 **Training Pipelines.** Our proposed method can be integrated with other base VLMs in MAS to
 1059 alleviate the multi-agent hallucination snowballing, requiring only one additional module for visual
 1060 relay selection. Following the typical training paradigm, we employ a two-stage training process
 1061 including a pre-training stage and instruction tuning stage, as reported in Table 10.

1066 D.2 ADDITIONAL RESULTS

1067 **Additional Analyses of Visual Relay Tokens.** To further validate the effectiveness of our selected
 1068 visual relay tokens in the visual flow, we conduct additional analyses with transformed visual fea-
 1069 tures and different combinations of subsets of vision tokens. Specifically, we employ an average
 1070 pooling, a two-layer MLP, and a lightweight transformer (Mehta et al., 2021) for visual token com-
 1071 pression, respectively. We also adopt object-level visual features (Neo et al., 2025), wherein we uti-
 1072 lize an external segmentation model (i.e., SAM2) and incorporate the vision tokens of the predicted
 1073 mask to relay visual information. Furthermore, we compare the results of different combinations of
 1074 vision token subsets, as defined in Table 1. These additional tokens are randomly selected from the
 1075 subsets, with the number of additional selections maintained below that of unimodal tokens.

1076 As presented in Table 11, uniformly compressed visual features fail to relay information among
 1077 agents and even exacerbate visual hallucinations due to vision transformation loss, particularly in
 1078 complex visual scenarios (e.g., in MMHal-Bench and HallBench benchmarks). Object-level visual
 1079 features also yield suboptimal performance, owing to obstacles in external information selection

1080
 1081 **Table 11:** Results of different transformed visual features or various combinations of subsets of
 1082 vision tokens as the visual flow to relay visual information, evaluated on LLaVA-NeXT-7B and cir-
 1083 cular structure. Due to the need for external model to obtain object-level visual features, we cannot
 1084 calculate the end-to-end latency of this method. “Perf.” indicates the quantitative performance on
 1085 the benchmark.

Visual Flow	CHAIR		POPE		AMBER		MMHal-Bench		HallBench	
	Perf.↓	Latency↓	Perf.↑	Latency↓	Perf.↑	Latency↓	Perf.↑	Latency↓	Perf.↑	Latency↓
Baseline	43.0	3.16	91.0	2.46	89.4	2.79	47.9	3.48	53.1	3.91
Compressed Visual Features (Pooling)	43.9	<u>3.33</u>	89.6	<u>2.61</u>	89.2	<u>2.95</u>	42.5	<u>3.64</u>	46.7	<u>4.05</u>
Compressed Visual Features (MLP)	42.7	3.40	91.6	2.73	90.4	3.02	44.9	3.77	51.8	4.18
Compressed Visual Features (Transformer)	42.2	3.61	91.9	2.96	91.1	3.27	48.5	3.99	53.3	4.40
Object-level Visual Features	42.5	-	92.3	-	91.8	-	47.2	-	53.4	-
(e) Unimodal + (a) Rise	41.0	3.55	92.7	2.87	92.1	3.20	<u>50.6</u>	3.87	<u>54.8</u>	4.33
(e) Unimodal + (b) Fall	42.0	3.56	92.3	2.89	91.3	3.22	<u>49.7</u>	3.88	<u>53.7</u>	4.34
(e) Unimodal + (a) Rise + (b) Fall	41.3	3.63	<u>93.1</u>	2.94	92.9	3.28	50.3	3.94	54.1	4.40
(e) Unimodal (Ours)	<u>41.2</u>	3.47	93.3	2.79	<u>92.7</u>	3.10	51.1	3.83	55.7	4.23

1096
 1097 and the introduction of additional latency. Additionally, unimodal vision tokens, adopted for visual
 1098 information relay, do not gain significant benefits from the integration of other vision token subsets,
 1099 while incurring extra time and computational overheads.

1100 **Correction Capability on Adversarial Visual Inputs.** We assess the correction ability of our ViF
 1101 in adversarial and noisy scenarios, including injecting edited images and mismatched images. The
 1102 former randomly masks the area in the image, and the latter directly inputs mismatched and wrong
 1103 image, both of them serve as strong adversarial scenarios. We stochastically inject the adversarial
 1104 image in the 2 to 4 agent turns, and assess the performance in the following 5, 10, 15, and 20 agent
 1105 turn, respectively.

1106 As depicted in Figure 10, our ViF exhibits superior correction capability over the baseline when
 1107 processing noisy and adversarial visual inputs, achieving by dynamically revising visual cognition
 1108 across agent turns rather than adhering rigidly to prior outputs. As mentioned earlier, base VLMs
 1109 in the multi-agent context tend to over-rely on prior texts to relay erroneous visual information.
 1110 Conversely, our proposed visual flow mitigates the propagation and snowballing of hallucinations,
 1111 thereby enabling enhanced correction and anti-adversarial capacities.

1112 **Combination with Other Hallucination Mitigation Strategies.** To further enhance the compati-
 1113 bility and applicability of our method, we evaluate the performance of combinations with existing
 1114 hallucination mitigation strategies, namely MemVR (Zou et al., 2025), VISTA (Li et al., 2025c),
 1115 FarSight (Tang et al., 2025b), DeCo (Wang et al., 2025), and TAME (Tang et al., 2025a). As com-
 1116 pared in Figure 11, we observe that most strategies achieve further improvements when combined
 1117 with our ViF in multi-agent environments.

1118 **Hyper-Parameter Analyses.** There are three key hyper-parameters in our proposed method, *i.e.*, the
 1119 salience of unimodal morphology ω when selecting visual relay tokens with unimodal distribution,
 1120 the temperature scaling τ in Equation 2, and the reallocation coefficient α_1 and α_2 in Equation 3 of
 1121 the middle and deep layers. As listed in Table 12, the lower the ω , the more proportions of visual
 1122 tokens would be included; however, excessive visual relay tokens will not bring extra performance
 1123 improvement but computation costs. When ω is set to 0.3, the model obtains the best results with
 1124 relatively less token overhead. Besides, as shown in Table 13, and Table 14, when τ , α_1 , α_2 are set
 1125 to 0.8, 0.1, 0.3, our model exhibits the greatest potential.

1126 **Efficiency Analyses.** As reported in Table 8, our proposed ViF incurs only marginal additional
 1127 computational overhead in respect of average latency and average number of operations. Addi-
 1128 tionally, as listed in Table 15, the computational overhead of our method remains relatively constant and
 1129 exhibits no substantial increase with higher resolutions.

1130 **Case Study.** As demonstrated in Figure 12, we visualize the generation procedure of the MAS
 1131 equipped with our proposed ViF on four selected samples from two benchmarks. We observe that
 1132 our method effectively mitigates the snowballing of multi-agent visual hallucinations, thereby en-
 1133 hancing overall performance. As shown in Example (b), although the agent outputs incorrect an-

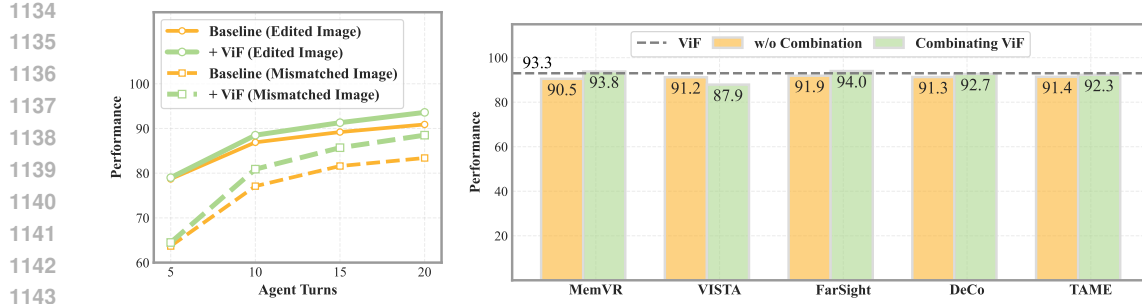


Figure 10: Analyses of correction ability on LLaVA-Next-7B and circular structure when feeding adversarial visual inputs, evaluated by POPE benchmark. Specifically, we incorporate five training-free methods, which are seamlessly integrated with our approach.

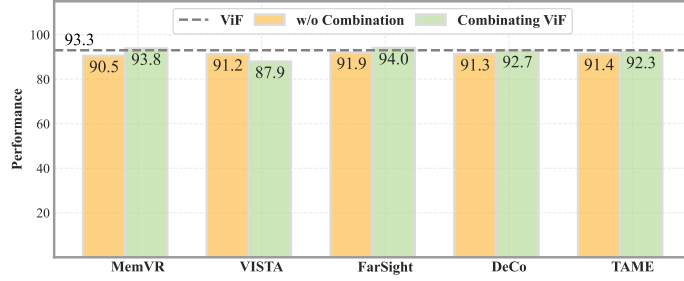


Figure 11: Comparisons of the combination of our proposed ViF and circular structure when evaluated by POPE benchmark. Specifically, we incorporate five training-free methods, which are seamlessly integrated with our approach.

Table 12: Influence of the salience of unimodal morphology ω on LLaVA-NeXT-7B and circular MAS structure.

ω	Ratio %	CHAIR↓	POPE↑	AMBER↑	MMHal-Bench↑	Hall-Bench↑	τ	CHAIR↓	POPE↑	AMBER↑	MMHal-Bench↑	Hall-Bench↑
0.1	17.6	44.5	90.2	88.6	45.9	52.7	0.6	44.1	91.4	90.8	48.2	52.1
0.2	6.7	42.8	91.5	89.2	49.1	52.8	0.7	43.0	92.4	91.8	50.3	54.2
0.3	2.3	41.2	93.3	92.7	51.1	55.7	0.8	41.2	93.3	92.7	51.1	55.7
0.4	1.3	41.7	92.5	92.0	49.8	54.9	0.9	41.0	93.1	92.2	48.9	53.8
0.5	0.2	42.9	91.1	89.6	47.9	53.0	1.0	41.7	92.5	91.6	47.7	52.8

Table 13: Influence of the temperature scaling τ on LLaVA-NeXT-7B and circular MAS structure.

α_1	α_2	CHAIR↓	POPE↑	AMBER↑	MMHal-Bench↑	Hall-Bench↑
0.0	0.2	43.2	89.6	89.1	47.2	47.6
0.0	0.3	42.8	90.0	89.3	47.4	48.2
0.0	0.4	43.0	89.8	89.0	47.1	47.8
0.1	0.2	41.3	93.1	92.6	50.7	55.3
0.1	0.3	41.2	93.3	92.7	51.1	55.7
0.1	0.4	41.8	92.9	92.4	50.5	54.9
0.2	0.2	42.9	90.6	89.2	47.3	48.1
0.2	0.3	43.1	89.8	88.5	46.9	48.0
0.2	0.4	42.9	89.6	88.9	46.5	47.7

swers regarding object detection in the first turn, subsequent turns still accurately identify the perceptual target through visual flow information. Furthermore, as illustrated in Examples (c) and (d), misunderstandings of visual information in images lead to erroneous semantic outputs in early agent turns; however, such errors are not propagated throughout the multi-agent procedure via the visual flow, thus suppressing the snowballing of visual hallucinations.

E LIMITATIONS

Although we conduct experiments on a total of ten models with different sizes, which verifies the robustness of compatibility of our proposed method, more experiments are still recommended. For example, the results on smaller size VLMs, *e.g.*, 3B, and also larger baselines, *e.g.*, 72B, could provide further evidence. Besides, the inclusion of more series of baselines, such as InternVL series (Chen et al., 2024b;a; Zhu et al., 2025), Llama 3 (Grattafiori et al., 2024), Ovis series (Lu et al., 2024; 2025), and MiniMCP (Hu et al., 2024), is also beneficial. Furthermore, more effective and

1188 **Table 15:** Efficiency comparison between our ViF and the base models on LLaVA-NeXT-7B and
 1189 the circular MAS architecture, which are evaluated with different image resolutions. We employ
 1190 the original-resolution samples from the CHAIR benchmark and conduct bilinear interpolation to
 1191 downsample them to 1/2, 1/4, and 1/8 of the initial resolution.

1192

Base Agent	1/8 Resolution		1/4 Resolution		1/2 Resolution		Original Resolution	
	Latency↓	FLOPs↓	Latency↓	FLOPs↓	Latency↓	FLOPs↓	Latency↓	FLOPs↓
Baseline	1.90	103.5	2.27	120.8	2.69	133.6	3.16	157.3
+Ours	2.17	112.2	2.57	130.0	3.01	143.8	3.47	168.5

1197

1198 **Example (a)**

1200 Are all of the cats the same
 1201 color?

1202 **Agent Turn 1:** There are many cats and they are in
 1203 different colors. 

1204 ...
 1205 **Agent Turn 2:** One is orange, two are grey, and two are
 1206 mixed ones, so they are not the same colors. 

1207 ...
 1208 **Agent Turn 3:** It is confirmed that their coats are
 1209 diverse, so the answer is no. 

1210 **Example (b)**

1202 Is there a toothbrush in the
 1203 image?

1204 **Agent Turn 1:** There is a cat on the sink, faucets, a
 1205 tissue holder, and a mirror. But there is no toothbrush.
 1206 So the answer is no. 

1207 ...
 1208 **Agent Turn 2:** There are some small pink and green
 1209 brush-shaped objects, typically found in toothbrush
 1210 cups beside sinks. So the answer is yes. 

1211 ...
 1212 **Agent Turn 3:** Those upright, rod-like objects matched
 1213 the shape and position of toothbrushes perfectly. So the
 1214 answer is yes. 

1215 **Example (c)**

1216 Do the persons live in this
 1217 house? Answer it and give the
 1218 rationale.

1219 **Agent Turn 1:** These people were dressed with great
 1220 refinement, and the man on the right holds a sword in
 1221 his hand, possibly a knight of noble birth. The decor of
 1222 the room was exceptionally lavish, perfectly matching
 1223 their attire. So they are likely live in the house. 

1224 ...
 1225 **Agent Turn 2:** The corridor was arranged with great
 1226 luxury and solemnity. And these people walked straight
 1227 ahead, with general clothing, as if they were on a tour or
 1228 being led, rather than moving about in a familiar house.
 1229 So the people probably don't live here. 

1230 ...
 1231 **Agent Turn 3:** Based on the way these people are
 1232 dressed and also their behavior and demeanor, they are
 1233 more like tourists. So they don't live here. 

1234 **Figure 12:** Case study of the results of ViF based on LLaVA-NeXT-7B across MM-Vet and POPE
 1235 benchmarks. For clarity, we choose the linear structure and the agent turn is set to 3.

1236

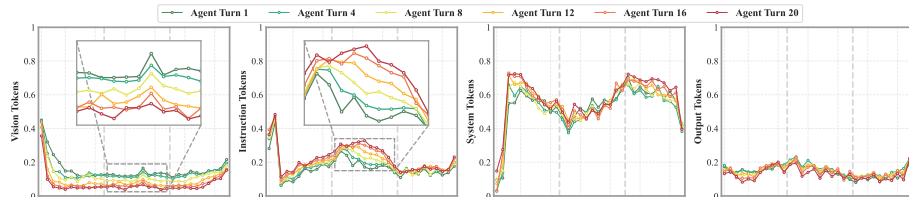
1237 complementary combinations of our ViF with other hallucination mitigation strategies, as well as
 1238 more optimal vision token selection, warrant further exploration.

1239

1240

1241

1242



(a) LLaVA-v1.5-7B

1243

1244

1245

1246

1247

1248

1249

1250

1251

1252

1253

1254

1255

1256

1257

1258

1259

1260

1261

1262

1263

1264

1265

1266

1267

1268

1269

1270

1271

1272

1273

1274

1275

1276

1277

1278

1279

1280

1281

1282

1283

1284

1285

1286

1287

1288

1289

1290

1291

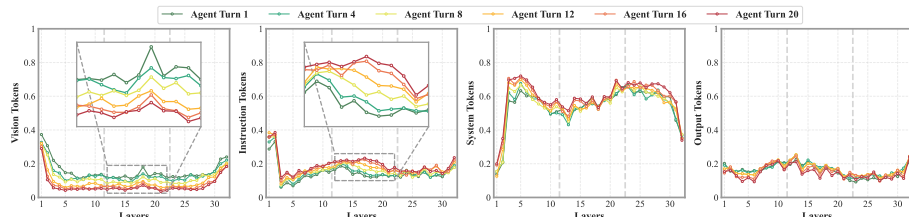
1292

1293

1294

1295

(a) LLaVA-v1.5-7B



(b) LLaVA-v1.6-7B

1251

1252

1253

1254

1255

1256

1257

1258

1259

1260

1261

1262

1263

1264

1265

1266

1267

1268

1269

1270

1271

1272

1273

1274

1275

1276

1277

1278

1279

1280

1281

1282

1283

1284

1285

1286

1287

1288

1289

1290

1291

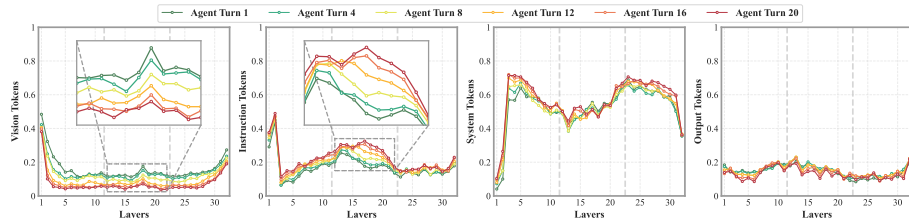
1292

1293

1294

1295

(c) LLaVA-NeXT-7B



(c) LLaVA-NeXT-7B

1260

1261

1262

1263

1264

1265

1266

1267

1268

1269

1270

1271

1272

1273

1274

1275

1276

1277

1278

1279

1280

1281

1282

1283

1284

1285

1286

1287

1288

1289

1290

1291

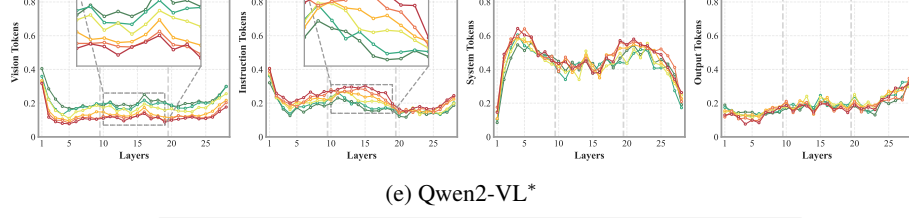
1292

1293

1294

1295

(d) LLaVA-OV-7B*



(d) LLaVA-OV-7B*

1270

1271

1272

1273

1274

1275

1276

1277

1278

1279

1280

1281

1282

1283

1284

1285

1286

1287

1288

1289

1290

1291

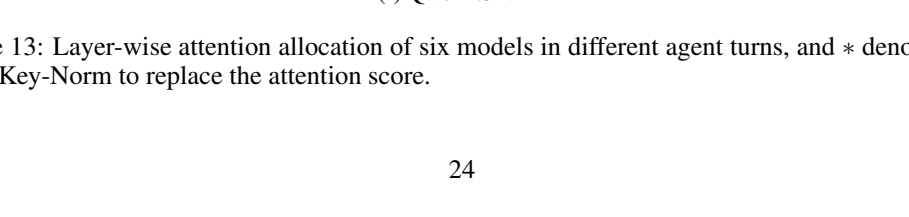
1292

1293

1294

1295

(e) Qwen2-VL*



(e) Qwen2-VL*

1286

1287

1288

1289

1290

1291

1292

1293

1294

1295

Figure 13: Layer-wise attention allocation of six models in different agent turns, and * denotes that using Key-Norm to replace the attention score.

1296 Table 16: Results of six VLMs when dropping different selected subsets of vision token in the
 1297 shallow, middle, and deep layers.

1298

		Shallow Layers				Middle Layers				Deep Layers			
		25%	50%	75%	100%	25%	50%	75%	100%	25%	50%	75%	100%
w/o Dropping													
LLaVA-v1.5-7B	(a) Random	49.1	41.3	36.1	28.7	77.3	64.1	60.2	56.2	81.6	81.1	80.6	80.2
	(b) Inactive	53.3	44.6	38.9	29.7	82.7	78.9	80.1	76.7	82.8	81.9	82.1	81.7
	(c) Rise	40.1	33.1	27.5	18.4	76.4	62.0	54.5	50.8	81.0	79.3	79.8	80.0
	(d) Fall	40.0	36.4	28.2	19.9	75.2	62.5	55.6	50.0	82.4	81.6	81.4	80.6
	(e) Unimodal	39.6	35.9	27.9	22.4	51.3	43.1	35.0	22.6	81.6	81.3	80.5	80.9
w/o Dropping													
LLaVA-v1.6-7B	(a) Random	49.9	42.2	37.2	28.0	77.0	63.6	60.1	58.1	81.8	81.1	80.7	80.9
	(b) Inactive	52.1	43.8	39.6	30.5	83.6	82.4	78.6	76.1	82.9	83.1	82.7	82.6
	(c) Rise	39.2	33.8	28.2	18.5	78.9	61.6	54.7	51.2	81.4	80.8	80.4	80.1
	(d) Fall	39.6	36.6	28.7	20.2	75.8	62.9	57.5	50.3	82.5	82.4	81.0	81.2
	(e) Unimodal	40.9	36.4	28.0	20.9	46.0	42.9	33.9	23.4	82.4	81.6	80.6	80.1
w/o Dropping													
LLaVA-NeXT-7B	(a) Random	51.8	44.5	38.4	30.5	78.9	66.1	62.7	59.0	84.4	83.2	82.9	82.6
	(b) Inactive	55.1	46.2	41.8	32.5	84.3	82.9	81.5	78.3	85.0	84.6	84.3	84.6
	(c) Rise	41.9	35.6	29.6	20.8	79.4	64.2	56.4	52.3	83.6	82.7	81.8	81.6
	(d) Fall	41.6	38.8	30.7	22.5	78.3	64.8	58.5	52.9	84.1	82.8	82.0	82.4
	(e) Unimodal	42.1	37.6	30.0	22.8	52.9	44.5	36.6	25.3	84.4	83.0	82.3	81.8
w/o Dropping													
LLaVA-OneVision-7B	(a) Random	52.7	45.1	41.4	33.2	82.4	72.5	66.8	63.7	87.5	86.6	86.2	86.5
	(b) Inactive	58.8	46.5	44.9	36.4	83.6	80.2	74.4	67.8	87.7	87.3	87.2	87.0
	(c) Rise	44.7	39.5	31.1	22.4	81.2	65.4	62.4	55.5	87.1	86.8	86.7	86.5
	(d) Fall	45.2	42.1	33.9	24.8	82.6	66.1	59.6	53.6	87.2	86.7	86.6	86.4
	(e) Unimodal	44.6	41.7	33.8	26.1	53.0	46.2	39.7	27.5	86.8	86.3	86.5	85.7
w/o Dropping													
Qwen2-VL-7B	(a) Random	53.2	44.7	39.8	31.2	79.3	67.1	62.6	59.0	84.8	84.0	83.5	83.0
	(b) Inactive	55.5	46.5	42.0	33.5	86.4	83.1	83.2	78.4	85.6	85.4	85.2	85.7
	(c) Rise	43.2	36.7	29.8	21.2	80.0	64.2	56.5	53.9	85.2	84.8	84.1	83.7
	(d) Fall	43.0	40.1	31.6	23.4	78.9	65.5	60.0	52.8	84.4	84.2	84.6	83.9
	(e) Unimodal	44.2	39.0	31.0	23.5	53.8	46.0	37.1	25.7	84.5	84.0	83.9	83.4
w/o Dropping													
Qwen2.5-VL-7B	(a) Random	51.5	44.8	39.2	31.2	80.0	66.3	63.9	59.5	84.4	83.9	83.6	83.4
	(b) Inactive	56.5	46.3	41.9	33.2	83.7	82.2	80.9	78.2	84.8	84.6	84.7	84.5
	(c) Rise	42.4	36.6	30.4	20.9	80.3	63.6	55.7	52.5	84.9	83.3	83.2	83.1
	(d) Fall	42.7	38.8	31.0	23.0	80.0	64.2	59.0	54.3	84.8	83.9	83.3	82.8
	(e) Unimodal	42.1	38.1	30.4	23.1	54.0	44.7	37.0	26.0	85.0	84.8	83.6	83.4

1324

1325

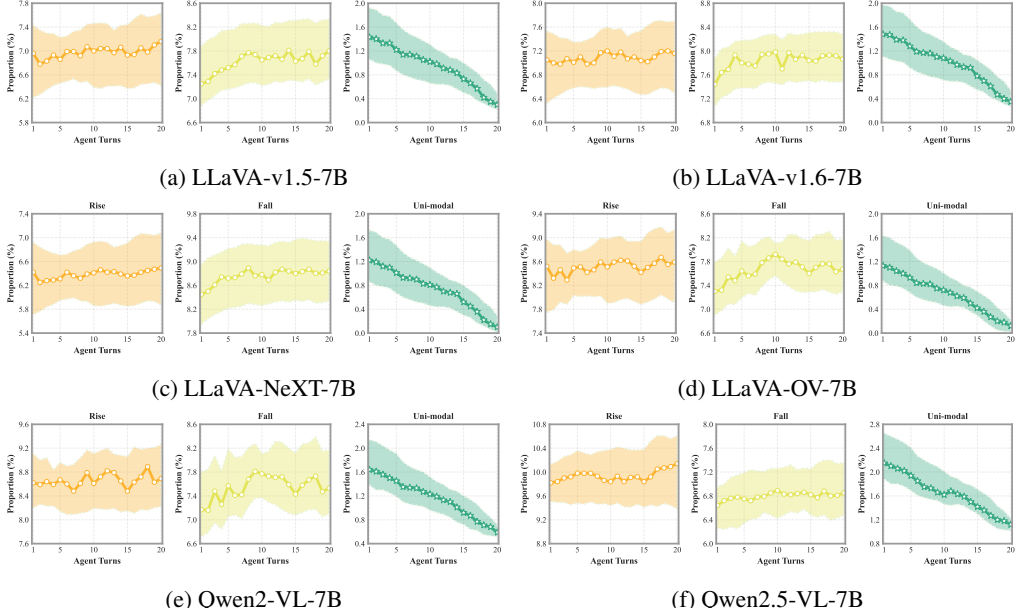


Figure 14: Proportion of vision tokens subsets of six models in different agent turns.

1346

1347

1348

1349

1350
 1351 **Prompt for Evaluating the Severity of Hallucination h**
 1352
 1353
 1354 You are a strict visual hallucination judge for vision-language models.
 1355 Your job is to evaluate the level of visual hallucination, given:
 1356 - 1. The user instruction and corresponding visual inputs.
 1357 - 2. The full generated output from the model.
 1358 - 3. The ground-truth of the instruction.
 1359 You must detect hallucinations and rate their severity on a 0 to 100 scale.
 1360 Definitions:
 1361 - A "visual hallucination" is: a class of hallucination phenomena in which a vision
 1362 -language model, conditioned on real visual inputs, generates visual details
 1363 in tasks that are inconsistent with, incorrect about, or entirely fabricated
 1364 beyond the given visual content, thereby making its outputs unfaithful to the
 1365 visual evidence. We care about hallucinations in both facts and reasoning.
 1366 Your tasks:
 1367 - 1. Decide whether the generated output contains visual hallucinations. (combining
 1368 visual inputs and ground-truth for verification)
 1369 - 2. If yes, briefly explain why they are hallucinations.
 1370 - 3. Output a SEVERITY score from 0-100 (integer).
 1371 Severity guidelines (0-100):
 1372 - 0: No hallucination. Fully consistent with references and context.
 1373 - 1-20: Very minor issues, local details, or small inaccuracies that do not change
 1374 the main conclusion.
 1375 - 21-40: Clear but localized hallucinations. The main conclusion is still mostly
 1376 correct.
 1377 - 41-60: Important hallucinations that significantly affect part of the answer or
 1378 core reasoning.
 1379 - 61-80: Severe hallucinations. The answer is largely incorrect or misleading.
 1380 - 81-100: Extreme hallucinations. The answer is almost entirely fabricated or
 1381 contradicts the references.
 1382
 1383
 1384
 1385
 1386
 1387
 1388
 1389
 1390
 1391
 1392
 1393
 1394
 1395
 1396
 1397
 1398
 1399
 1400
 1401
 1402
 1403